Part 1

Methodological Bases

1

Extraction and Segmentation of Structures in Image Sequences

1.1. Problematics

The analysis of imaged anatomical or biological structures and of their dynamics is an important task in terms of application and therefore of diagnostics. This analysis facilitates the quantification of the shape of these structures and their possible evolution over time, whether this evolution is intrinsic to the functioning of the structure (cardiac motion for example) or indicating a transformation related to a pathology (tumor evolution).

Such an analysis involves in the first place the extraction of these structures from the acquired images according to a given modality, which corresponds, in image processing terminology, to a segmentation phase. This chapter is devoted to this problem: after a very brief overview of the existing techniques, it discusses in detail the methodology of deformable models and more specifically their more flexible form, namely variational active contours. The chapter concludes with specific examples for the application of this type of technique carried out in the field of cardiac ultrasound imaging.

1.2. Overview of segmentation methods

Segmentation is a fundamental operation in imaging and cardiac and thoracic imaging in particular. Its role consists of assigning to the parts of an

---

Chapter written by Olivier BERNARD, Patrick CLARYSSE, Thomas DIETENBECK, Denis FRIBOULET, Stéphanie JEHAN-BESSON and Jérome POUSIN.

image a relevant category ("muscle", "blood", "tumor", etc.) relating to the underlying medical application: detection of the presence/absence of a pathological structure (for example "tumor", "aneurysm"), evaluation of the area, the extent, the volume of organs or the pathological structures as well as their evolution over time. Due to this central role, image segmentation is a very active area of research. This can be illustrated by observing the result of a search on the Web of Science® (Figure 1.1) and based on the presence of the terms "image segmentation" in the title of articles over 15 years (1994–2009). It can be seen that more than 4,700 articles[1] have been published during this period and that this number is constantly increasing.

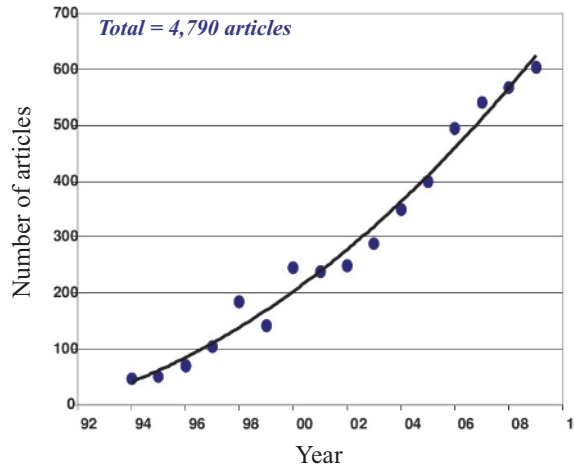

Figure 1.1. *Number of articles containing the terms "image segmentation" in the title for the period 1994–2009*

A segmentation method can be schematically characterized by three main elements (see Figure 1.2): (1) the low level properties (or "image information") used to characterize the objects to detect, (2) *a priori* knowledge introduced to constrain the segmentation and (3) the formalism chosen to integrate these two pieces of information.

1 It should be noted that these figures likely provide an underestimation of the actual number of articles related to this theme, where research has been restricted to the titles of articles.

If only the "image information" aspect is considered, segmentation can be formally defined as an operation consisting of partitioning the image in related regions verifying a consistency predicate, based for example on statistical properties or on texture. Segmentation can also be carried out according to a dual approach by considering the differences between these regions: two adjacent regions must actually present significant variations of properties along their common border. These variations can be quantified using conventional differential operators (for example, the amplitude of the gray level gradient) or more sophisticated techniques such as the phase-based approach developed by [MUL 00]. Following these definitions, segmentation methods are conventionally qualified as "region-based approaches" or "contour-based approaches".

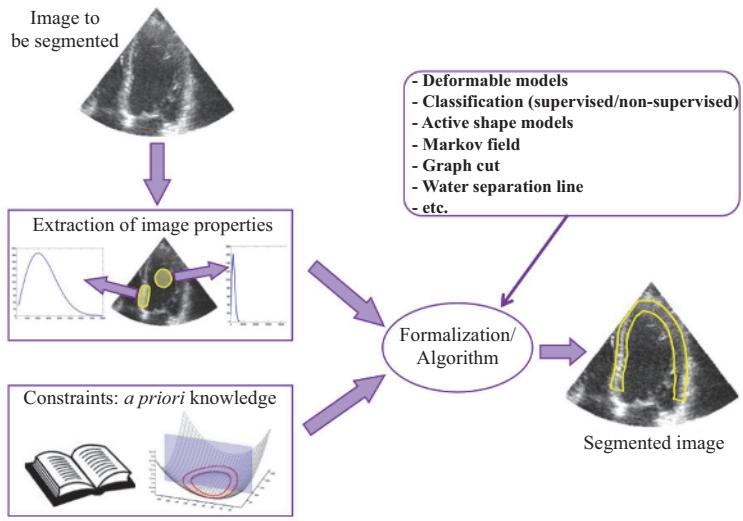

Figure 1.2. *General outline of a segmentation approach*

Due to imperfections presented by images (i.e. noise, occlusions, lack of contrast, etc.), to perform a segmentation using only the region or contour characteristics previously referred to reveals itself in most cases to be difficult, if not impossible. That is why *a priori* knowledge is usually introduced, relative to the intrinsic properties of the object to be detected, such as its shape, its grayscale distribution or its motion when it comes to image sequence. This knowledge may be purely abstract (for example "the form of the object must be smooth") or built from the statistical analysis of a training set representative of the images to process. Once established, these *a*

priori must be formalized and incorporated as constraints in the segmentation process. It is worth noting that the majority of the constraints used refer to the shape of the objects to segment.

These two types of information – image properties and *a priori* constraints – must then be integrated into a common formalism, itself numerically implemented as an algorithm. The importance of image segmentation research, highlighted above, has led to the development of many approaches, such as active contours, active shape models (ASM), approaches by classification, Markov fields, etc. We will focus in this chapter on one of the most important approaches in cardiac and thoracic imaging, namely deformable models.

1.3. Summary of the different classes of deformable models

Deformable models constitute a dominant approach to segmentation. They were originally introduced by Kass *et al.* [KAS 88] with the "snakes model" and quickly found applications in medical imaging. This significance relates to the fact that their formulation is very flexible, allowing the integration of many types of image properties and *a priori* constraints. As such, the literature concerning deformable models is highly significant and in this introductory section, we consider very synthetically two broad classes of approaches:

– energy-based approaches: the energy reflecting the properties of the object to segment (gray levels, shape, etc.) and expressed in terms of the deformable model (position and shape) is built. The segmentation process then corresponds to the minimization of this energy;

– in contrast, "non-energy-based approaches" do not involve energy directly dependent on the model. It should be noted that if some of these methods make use of a criterion minimization stage, it is therefore not expressed directly as a function of the deformable model (thus, for example, "atlas approaches" perform a registration step by minimizing a similarity criterion).

Following this section, we will detail more particularly two deformable model approaches: deformable templates (DTs) in section 1.4 and variational active contours in section 1.5.

1.3.1. *Non-energy approaches*

1.3.1.1. *Active shape models*

ASMs were originally described by Cootes in 1995 [COO 95]. This approach can be seen as a method of deformable models incorporating intrinsically an *a priori* on the shape of the object to segment, this *a priori* being built using a statistical representation of the space of the eligible shapes.

In practice, this representation is constructed from a training set of images, where contours are manually plotted, aligned and sampled on N points. This step enables the construction of a model of distribution of contour points from which shape statistics are established by using principal component analysis (PCA), which provides the average shape and the K main variation modes of this shape. The object to segment is then detected by iteratively deforming an initial contour: each of the N points of this outline is shifted in order to move it closer to the edge of highest amplitude located in its neighborhood. This set of displacements provides a new set of points that is projected onto the K main variation modes: the new shape obtained is thus forced to belong to the space of eligible shapes defined by these modes. This process is iterated until convergence, namely when the displacements can be considered as negligible.

Active appearance models (AAMs) constitute an extension of the ASMs [COO 01]. In this approach, the constraint concerns not only the shape but also the appearance, defined as the average and the principal variation modes of the normalized gray levels of the region corresponding to the reference contours. An example of the application of this technique in echocardiography can be found in [BOS 02].

1.3.1.2. *Atlas-based approaches*

The basic principle of atlas-based segmentation is conceptually simple. An atlas corresponds to a pair made of an image of a given modality and its segmentation, represented by a set of labeled regions. This segmentation is most often obtained by performing a manual outline. The segmentation of a new image of the same modality is then performed in two stages. The atlas image and the new image are first mapped using a registration algorithm, which uses the local properties of these images (from gray levels). Thus, this registration phase provides, on output, the transformation that allows us to map the “atlas image” to the new image. This transformation is then applied to the labeled regions of the atlas, thus providing the new image segmentation.

Within this framework, the different approaches of atlas segmentation are distinguished by the type of registration used, namely by the type of

transformation (affine, rigid, nonlinear, etc.) and the similarity measure (absolute differences, mutual information, etc.) implemented in the algorithm. Another important feature lies in the construction and use of the atlas: if the base method considers a single atlas, a number of authors have proposed to improve the method either by using an average atlas, or by selecting the atlas best suited to the new image in a base of atlases. Any reader wishing to deepen their knowledge on the technical aspects of atlas segmentation can usefully consult some general articles such as [ROH 05] and [RAM 10].

1.3.1.3. *PDE-based approaches*

As a first step, some approaches that make use of deformable models have been developed based solely on the definition of the evolution equation without necessarily going through energy minimization. We will call these methods "PDE-based approaches" because they share the use of a geometric partial differential equation (PDE) to define the evolution of an active contour. These have notably originated conventional approaches such as an "active contour" presented in detail in section 1.5. Thus, Malladi *et al.* [MAL 95] and Caselles *et al.* [CAS 93] have introduced as a first step geometric active contours for which the evolution speed of the contour is defined based on intrinsic properties of the image such as the gradient and on geometrical properties of the curve such as curvature. Active contours driven by the balloon force introduced by Cohen *et al.* [COH 91] also fall within this framework. However, in a seminal work, Ronfard [RON 94] defines an evolution equation based on the characteristics of the internal and external regions of the edge thus resulting in a first PDE based on the characteristics of the regions and not anymore simply on the gradient of the image. We will also quote in this section Gradient Vector Flow-based approaches (GVF-based approaches) by Xu and Prince [XU 98] even if the principle is very different. In this type of approach, a contour displacement field is precomputed and used as additional velocity to the *snakes* model proposed by Kass *et al.* [KAS 88].

1.3.2. *Energy-based approaches*

1.3.2.1. *Variational approaches*

Deformable models based on the variational approach are most often called "active contours" and constitute the most frequent form of these models. Variational active contours are characterized by an energy functional, whose minimum corresponds to the required segmentation (hence the term variational): thus the object to be detected is segmented by iteratively distorting an initial contour (or a 3D surface), in such a way that this

evolution decreases the energy until it reaches a minimum. In two dimensions, this approach translates into the evolution of an initial curve in an image toward the structure to segment (Figure 1.3).

An important characteristic of this approach lies in the fact that the evolution leading to a minimum can be obtained systematically by standard variational calculation (i.e. Euler-Lagrange equations or Gâteaux derivatives) or by using shape gradients. The implementation of the variational active contours for a given application passes in practice through the following steps and choices:

– choice of the representation of the active contour (see Figure 1.5, sections 1.5.1.2 and 1.5.1.3). This representation may be explicit, or most often parametric or implicit;

– formulation of the energy functional. This step depends on the application, since the functional should be constructed so that a local minimum is associated with the border of the object to be detected;

– obtaining the evolution equation. This step involves the calculation of the variational derivative of the functional (Euler-Lagrange's equations or Gâteaux derivative) or of the associated shape gradient. This equation consists formally of a PDE.

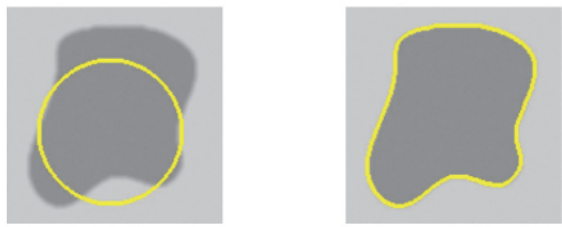

Figure 1.3. *Active contour segmentation principle. The initial contour a) is distorted to detect an object in an image b). For a color version of this figure, see www.iste.co.uk/clarysse/cardiac.zip*

The technical aspects of implementing these stages are described in section 1.5. Section 1.6 details the different approaches used to introduce the shape and motion constraints in this formalism and section 1.7 provides examples of the implementation of this approach in the context of 2D and 3D echocardiographic imaging.

1.3.2.2. *Dual approaches*

The use of dual approaches [CHA 99, CHA 04, AUJ 05] and of tools borrowed from convex optimization is one of the current alternatives to conventional minimization methods through the use of a PDE resulting from Euler-Lagrange's equations. These minimization algorithms thus present the advantage of being generally more effective in terms of calculation costs and above all, they facilitate obtaining the global minimum (or minima). They are based on the duality theory and convex optimization and they therefore require the transformation of the initial optimization problem into a convex research problem of an optimal u function. With regard to the particular case of segmentation, instead of searching for an optimal domain (the search space being non-convex), the approach consists of searching for a functional u belonging to the space of bounded variation functions. The optimal function u^* will then be thresholded in order to split the image into two optimal areas with regard to the considered criterion. In a first approach, Nikolova *et al.* [NIK 06] have proposed this methodology by providing a first convex resolution of the Chan and Vese's model [CHA 01]. Then the works of Bresson *et al.* [BRE 07] helped to highlight the existing relationship between models based on the minimization of the total variation and geodesic active contours. Problematics related to these approaches exist in the choice of the threshold to find the final segmentation and also in the convexification of the initial criterion (it should be noted that a recent solution has been proposed in [BRO 12]). A large number of approaches explore dual methods in applications such as noise removal or restoration. Among the approaches that use dual-based segmentation approaches for medical imaging, [WOJ 10] can be cited, for example, where applications concerning the segmentation of PET-CT multimodal images of the thorax were studied.

1.3.2.3. *Discrete approaches*

We will here mention briefly various segmentation techniques that make use of discrete representations to solve PDEs. Some approaches propose to use properties in graphs after optimization (example [BOY 06]). Other more recent approaches directly reformulate the criterion or the PDEs on discrete structures such as graphs using equivalences between continuous and discrete formulations. These equivalences can be carried out either by combinatorial approaches or by finite difference calculations. Thus, Grady *et al.* [GRA 08, GRA 09] propose to completely reformulate some segmentation criteria used in the context of deformable models (including that of Chan and Vese [CHA 01]). Their approach is based on the reformulation of the various derivation operators by using combinatorial analogs of differential operators. One of the difficulties of these approaches lies in the discrete mapping of the

different continuous variables and in the definition of a representation of "a contour" which can be used in practice with its attributes (length, curvature, etc.). The proposed approaches are effective in terms of computation times because they can take advantage of the arsenal of combinatorial optimization tools. They can also be generalized for the use of abstract data (pixels can then be replaced by patches for example or other more complex data). Other approaches are based on the reformulation of the derivation operators by calculations of finite difference in graphs [ELM 08]. The advantage of these approaches is to provide a discrete formulation of the PDEs and to facilitate the processing of arbitrary topology graphs. A reformulation of a number of segmentation PDEs was notably introduced in [TA 01, DES 11]. Finally, we will also mention the use of discrete geometry tools in order to redefine the deformable models [LAC 05].

1.3.2.4. *Deformable templates*

Deformable templates (DTs) have been introduced with some success as a generic approach for the recognition of shapes in computer vision. The *a priori* shape is described by a "standard" representation of the geometry called a "template". The adaptation of the template to the object present in the image is performed by the iterative and oriented modification of the parameters of the template guided by the optimization of a matching measure. As we will see in the next section, a DT can integrate, besides a geometric representation relating to the location and to the shape, information related to the texture or the material.

1.4. Deformable templates

DTs are parameterized models that exhibit a real significance when an *a priori* geometric shape of the object to segment is available. They have shown some success for tasks of shape detection and recognition [JAI 96, YUI 91]. A DT consists of a reference template that describes the most standard geometric shape of the object, of a transformation function that drives the variation of the template reference (geometric shape) and of a matching measure of the deformed template to the image information. The transformation of the template is even easier if it is represented by a small number of parameters, but *a contrario*, too low a number of parameters limits the diversity of the representable shapes. The analytical DT describes the reference template by a set of analytical curves (example: ellipses). This implies that the object to detect presents a representable shape by means of the variations of the limited number of parameters that describe it (example: the parameters of an ellipse) [JAI 98]. The reference template can also be

defined by a "standard" parameterized prototype that describes the average shape or the more likely one, and by a transformation function acting on the parameters (in a permissible range) to generate variations in the prototype. DTs interacts with the image and its primitives in order to dynamically adjust the parameters of the model with respect to the force fields originating in the image. Many variants have been proposed taking into account the different possible choices to represent the prototype (polygons, Fourier representations, B-splines, grayscale images, etc.) and the transformation process (Markov processes, maximum likelihood, maximum *a posteriori*, cost function optimizations, etc.) [JAI 98]. The prototype can be built from the learning techniques implemented in the active shape and appearance models. Several methods rely on a probabilistic and statistical formulation of the transformation. Allasoniere *et al.* offer a mathematically coherent statistical framework in terms of probability model and of the estimation process of the template (existence and consistency) [ALL 07].

In the context of cardiac imaging, a geometric DT was proposed by Rueckert and Burger where the contours are defined by a set of points-vertices in rest and deformed configurations. The segmentation is then obtained by the maximization of an *a posteriori* probability which combines internal energy limiting the non-affine deformations (bending energy of the model) and external energy based on edge maps [RUE 97]. Vincent *et al.* introduced the elastic DT (EDT), which establishes a coupling between internal and external contours (endocardium and epicardium) by means of the elasticity equations [VIN 99, VIN 00, VIN 01]. As the matter of fact, the objective consists of taking into account the physical nature of the myocardium with the purpose of tracing the deformation information not only concerning the walls but also concerning the myocardial tissue throughout its thickness. We present the EDT model, its implementation and its various extensions in the next section.

1.4.1. *Elastic deformable template principle*

The elastic DT model is a combination of an *a priori* reference model made of a collection of triangular elements in 2D or tetrahedral elements in 3D. Interior and edge vertices are labeled differently. The deformation of the EDT is governed by elasticity equations (internal energy) and a fitting measure of the model to the image data (external energy). The resulting segmentation is obtained from the deformation of the initial template translated by the displacement $\mathbf{u}$ applied to the vertices and resulting from the minimization of the functional J:

$$J = \min_{u} \left(J_{elastic}(\mathbf{u}) + \lambda J_{image}(\mathbf{u}) \right) \qquad [1.1]$$

where u represents the displacement to be applied to the model and λ a scalar that achieves the balance between the two terms. Elastic internal energy is expressed from the tensors with constraint σ and deformation E, itself linked to the displacement by $\mathbf{E}(\mathbf{u}) = \frac{1}{2}\left(\boldsymbol{\nabla}\mathbf{u} + \boldsymbol{\nabla}\mathbf{u}^T + \boldsymbol{\nabla}\mathbf{u}^T\boldsymbol{\nabla}\mathbf{u}\right)$:

$$J_{elastic}(\mathbf{u}) = \frac{1}{2}\int_{\Omega} trace\left(\sigma\mathbf{E}^T\right) d\Omega \qquad [1.2]$$

where Ω is the domain of the reference model at rest. The external energy characterizes the work of forces $\mathbf{f}$ originating in the image on the vertices of the model (reduced to the edges):

$$J_{image}(\mathbf{u}) = \int_{\Gamma} \mathbf{f}\cdot\mathbf{u}\, d\Gamma \qquad [1.3]$$

where Γ is the edge of the domain Ω. It is expected that for the minimum of this energy, the edge is superimposed on the contours of the object where the forces, calculated by an operator such as a gradient for example, are minimal while limiting the elastic deformation of the reference model. The energy J is approximated by the finite elements method (FEM) from the tiling of the area with M 2D triangular or 3D tetrahedral elements. The displacement in each element of the model is represented by a combination of linear functions (taking the value 1 in one of the vertices and 0 for the other vertices) and of the displacements to the vertices of the element [VIN 01]. The functional J in this case is rewritten in the quadratic matrix form as:

$$J(\mathbf{U}) = \frac{1}{2}\mathbf{U}^T\mathbf{K}\mathbf{U} - \mathbf{U}^T\mathbf{F} \qquad [1.4]$$

where $\mathbf{U}$ and $\mathbf{F}$ respectively are the displacement and force vectors to the nodes (of dimension $M \times 2$ in 2D, $M \times 3$ in 3D), $\mathbf{K}$ the stiffness matrix (incorporating the material properties via Young's modulus and Poisson's ratio). The assembly of the matrix $\mathbf{K}$ is based on the superposition principle of the stiffness matrices of all of the elements [VIN 01]. The optimality condition for J is written as $\nabla J(\mathbf{U}) = 0$, that is:

$$\mathbf{K}\mathbf{U} - \mathbf{F}(\mathbf{U}) = 0 \qquad [1.5]$$

Taking into account the dependency of $\mathbf{F}$ with regard to the displacement, the solution of equation [1.5] is obtained as the stationary solution (or asymptotic in time) of:

$$\frac{\partial\mathbf{U}}{\partial\tau} + \mathbf{K}\mathbf{U} = \mathbf{F}(\mathbf{U}) \qquad [1.6]$$

with τ an evolution parameter.

1.4.2. *Dynamic elastic deformable template*

The goal being the assesment of the dynamics of the heart in a sequence of images, Schaerer *et al.* have proposed a spatiotemporal version of the EDT integrating continuity and periodicity constraints [SCH 08, SCH 10]. The dynamic EDT model is based on a simplified dynamics equation:

$$\mathbf{D}\dot{\mathbf{U}} + \mathbf{K}(\mathbf{U})\mathbf{U} = \mathbf{F}(\mathbf{U}, t) \qquad [1.7]$$

where damping $\mathbf{D}$ will be represented by a single scalar α. Continuity and periodicity are introduced considering that force and displacement fields are defined on a space of Fourier functions. Thus, the force field $\mathbf{F}$ will be written as a linear combination of these basic functions:

$$\mathbf{F}(t) = \sum_{l=-\frac{N}{2}}^{l=\frac{N}{2}} f^l \, e^{i2\pi \, l \, t} \qquad [1.8]$$

N defines the number of harmonics and therefore has the effect of regularizing the field (the larger the N is, the more the solution can present oscillations). The solution (dynamic displacement field) is obtained as in the static case, with a pseudo-unsteady schema:

$$\begin{cases} \frac{\partial \mathbf{U}}{\partial \tau} = \mathbf{F}(\mathbf{U}) - \mathbf{A}\mathbf{U} \\ \mathbf{U}(0) = 0 \end{cases} \qquad [1.9]$$

with the operator $\mathbf{A} = \alpha \frac{d}{dt} + \mathbf{K}$. The implementation uses finite differences for the temporal schema:

$$\left(\frac{1}{\Delta\tau} + \frac{\alpha}{\Delta n} + \mathbf{K} \right) \mathbf{U}_n^\tau = \mathbf{F}\left(\mathbf{U}_n^{\tau-1}\right) + \frac{1}{\Delta\tau}\mathbf{U}_n^{\tau-1} + \frac{\alpha}{\Delta n}\mathbf{U}_{n-1}^\tau \qquad [1.10]$$

where τ is an evolution parameter, n is the time index and $\Delta\tau$, Δn are the corresponding steps.

The iterative minimization of equation [1.10] leads to the simultaneous adjustment of the template throughout the sequence of images which ensures the physical consistency (imposed by the equations of elasticity) between the successive phases of the motion relative to an individual phase-by-phase segmentation. The resulting model also directly provides parameters related to the deformations of the object (of the myocardium in the case of heart images).

1.4.3. *Elastic deformable template and modal analysis*

The EDT model can be compared to Sclaroff and Pentland's modal shape representation, which quantifies the difference/similarity between shapes by means of a modal deformation energy [SCL 95]. The matrix $\mathbf{K}$ being symmetric semidefinite positive is diagonalizable. The equation $\mathbf{KU} = \mathbf{F}$ can be rewritten on the basis of the eigenvectors, also called eigenmodes of $\mathbf{K}$:

$$\tilde{\mathbf{K}}\tilde{\mathbf{U}} = \tilde{\mathbf{F}} \qquad [1.11]$$

with $\tilde{\mathbf{K}} = \mathbf{P}^{-1}\mathbf{K}\mathbf{P}$, $\tilde{\mathbf{U}} = \mathbf{P}^{-1}\mathbf{U}$, $\tilde{\mathbf{F}} = \mathbf{P}^{-1}\mathbf{F}$ and $\mathbf{P} = (\mathbf{V}_1, \cdots, \mathbf{V}_M)$.

The three (respectively six) first eigenmodes correspond to the three (respectively six) degrees of freedom of the rigid motion of a 2D (respectively 3D) object. The eigenvalues and thus the elastic energy of the motion associated with these modes are zero. The elastic energy associated with the following modes increases with their rank. An eigenmode with a high rank shows high spatial frequencies. Unrealistic shapes can be eliminated by the removal of some eigenmodes in a manner similar to the limitation of the number of Fourier harmonics exploited in the dynamic EDT (see above). This principle can be extended to the contraction motion of the heart. This is what was initially suggested by Vincent *et al.* without having the necessary *a priori* knowledge at the time [VIN 01]. Since then, Remme *et al.*, for example, have selected and estimated nine eigenmodes (with principal component analysis) of the global variations of the epicardial and endocardial surfaces between the heart end-diastole and end-systole and have shown that a patient group and a control group could be differentiated from the average values of these modes [REM 04].

1.4.4. *The elastic deformable template in practice*

The processing of a sequence of images requires the positioning of the reference template in an image of the sequence (usually the first) and the adjustment of the model parameters. This will be illustrated in the segmentation and the dynamic monitoring of the left ventricle (LV) in a cine magnetic resonance imaging (MRI) sequence with short-axis orientation. This type of acquisition is common in cardiac MRI and produces a time series of images (typically 20-60 images) at a given heart level. The initialization of the model (here a ring) is performed either manually by designating three points of the endocardium and one point belonging to the epicardium, or automatically by recognition of the LV cavity and the average thickness of the

myocardial wall. The parameters of the EDT to define are Young's modulus (between 0.1 and 0.5), Poisson's ratio (between 0 and 0.5, usually set to 0.2), the number of image resolution levels, the number of harmonics (generally fixed to 5), the stopping criterion (which corresponds to the difference between two successive solutions of the unsteady schema, value in the range of 10^5) and a contraction parameter (usually set at 0.2). In practice, in the case of cardiac MRI segmentation, experiments carried out particularly in the context of segmentation competitions (MICCAI 2009 notably, on 45 multislice cine MRI data sets [RAD 09]) have shown that Young's modulus is the only parameter to really adjust [SCH 10].

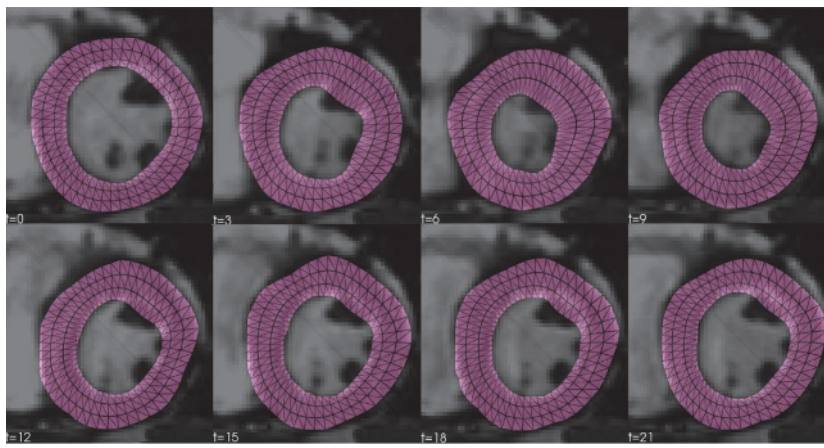

Figure 1.4. *Results of heart segmentation in a cine MRI image sequence in short-axis orientation covering the cardiac cycle. The EDT is superimposed on the image with light transparency. It is made up of triangles arranged in three layers. For a color version of this figure, see www.iste.co.uk/clarysse/cardiac.zip*

Figure 1.4 shows a result obtained from a dynamic sequence in short-axis cine MRI. The evaluation has also shown that dynamic EDT was one of the few models that allows for jointly segmenting the endocardium and the epicardium across a dynamic series and that the results in terms of physiological parameters (ejection fraction, mass and volume) are in the average of the semi-automatic methods [SCH 10]. The algorithm obtains good results for epicardial contours. Dice's criterion for cases treated on-site is still greater than 0.9 for the outer edges, and 0.85 for the inner edges. The average perpendicular distance relative to a reference for the endo- and epicardial contours is about 3 mm, regardless of the data set. These evaluations have been carried out in the context of the working group

IMPEIC/MediEval of the GDR Stic-Santé[2]. Elements comparatively to other methods are given in Chapter 5, dedicated to the evaluation of segmentation methods. The main recent developments of the dynamic EDT relate to the prescription of anchor points, designated by the user and intended to impose passing points in challenging cases [CAS 10]. It is also possible to introduce an anisotropy in the deformation controlled by local directions (myocardial fiber orientation) as shown by the preliminary findings reported in [STO 12]. Furthermore, EDTs provide quantified information about the motion of the heart through maps of the principal circumferential and radial deformations of clinical interest [CAS 12].

1.5. Variational active contours

As this has been previously mentioned, the implementation of variational active contours for a given application goes in practice through the following steps:

– choice of the representation of the current contour. This representation is most often parametric and implicit, but explicit expressions have recently been used;

– formulation of the energy functional. This step depends on the application: the functional should be designed so that a local minimum corresponds to the border of the object to be detected;

– derivation of the evolution equation in order to move the current contour from its original form (most often supplied by a manual tracing) to the desired segmentation. This stage involves the calculation of the variational derivative of the functional (Euler-Lagrange equations or Gâteaux derivative) or the derivation of the associated shape gradient. This equation consists formally of a PDE.

These different aspects are detailed in this section.

1.5.1. *Active contour representations*

We express here the active contour formulation in 2D, which allows the writing to be simplified. It should be noted however that generalization in any dimension is immediate in the case of implicit and explicit representations.

2 http://stic-sante.org/.

The term "active contour" is then unsuitable and it is therefore preferable to use the more general term of interface.

1.5.1.1. *Parametric representation*

Parametric representation has historically been the first used for the modeling of active contours in the context of a segmentation problem [KAS 88]. The contour simply corresponds to a parametric curve $\Gamma(s) = (x(s), y(s))$ defined by $[0, 1] \rightarrow \mathbb{R}$ with s representing the curvilinear abscissa (see Figure 1.5(a)).

1.5.1.2. *Implicit representation and level set*

Define Ω as the subset of $\mathbb{R}^2$ corresponding to the spatial domain of the considered image. The active contour Γ constitutes the boundary of an inner region that we will denote Ω_{int}. The exterior region will be denoted as Ω_{ext} with $\Omega_{\text{ext}} = \Omega \setminus \Omega_{\text{int}}$. In the formalism of level sets, the active contour is represented by means of an implicit function, namely as the zero level of a Lipschitzian function of $\mathbb{R}^2$ (see Figures 1.5(b) and 1.6). We will designate by $\phi(\mathbf{p})$ this function, with $\mathbf{p} = (x, y)$ representing a point of Ω. This function verifies:

$$\begin{cases} \phi(\mathbf{p}) > 0, & \forall \mathbf{p} \in \Omega_{\text{int}} \\ \phi(\mathbf{p}) < 0, & \forall \mathbf{p} \in \Omega_{\text{ext}} \\ \phi(\mathbf{p}) = 0, & \forall \mathbf{p} \in \Gamma \end{cases} \qquad [1.12]$$

Historically, level sets methods have been introduced in physics by Osher and Sethian [OSH 88] to solve front propagation problems. The use of this formulation in segmentation was, however, initially proposed by Caselles *et al.* [CAS 97] and almost simultaneously by Yezzi *et al.* [YEZ 97].

The significance of this representation has its origins in the fact that parametric formulation of active contours has the disadvantage of not easily managing objects with a complex topology (objects with holes or comprising several components for example). The representation of the contour by level sets on the contrary allows an easier management of this type of shape due to its implicit nature (see Figures 1.6 and 1.8 for an example of evolution). As we will see later on, the implicit representation of the interface also presents other advantages: it facilitates the discretization of the evolution equation on a regular grid, its expression is immediately generalized in any dimension and it facilitates the introduction of evolution terms depending on regional properties of the image.

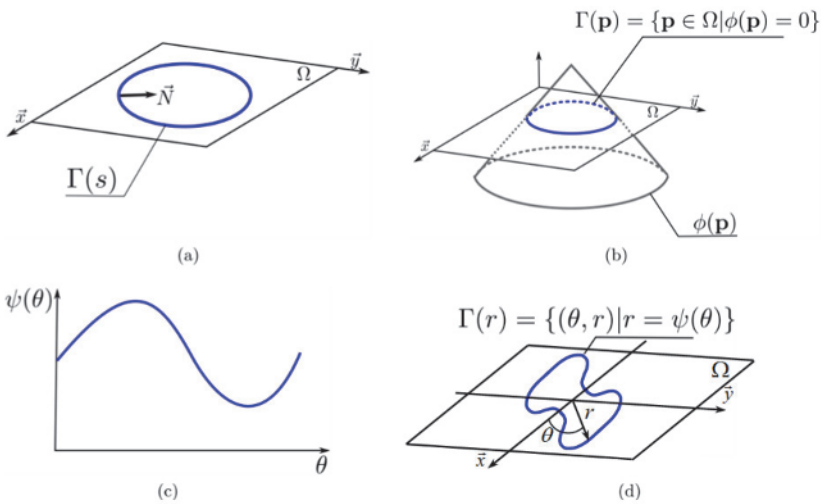

Figure 1.5. *Contour representations. a) Parametric representation. b) Level set representation: the contour corresponds to the level zero of the implicit function $\phi(\mathbf{p})$. c) and d) Explicit representation: the contour Γ corresponds to a set of points for which one of the coordinates (r) is given as a explicite function of the remaining coordinates (θ). For a color version of this figure, see www.iste.co.uk/clarysse/cardiac.zip*

1.5.1.3. *Explicit representation*

The interface Γ can also be represented using an explicit function. Geometrically, this implies for each point of the interface that one of the coordinates is expressed with respect to the other coordinates. In the 2D case, this is written as follows: $\Psi : \mathbb{R} \rightarrow \mathbb{R}$, $x \mapsto \Psi(x)$ (see Figures 1.5c and 1.5d). The contour corresponds to the set of all points for which $y = \Psi(x)$. A link with the implicit representation seen above can be easily established by defining a function in Ω such as:

$$\phi(x, y) = \Psi(x) - y \qquad [1.13]$$

The contour can then be represented as $\Gamma = \{\mathbf{p} = (x, y) \,|\, \phi(\mathbf{p}) = 0\}$. It is worth noting that in the case of explicit representation, a coordinate system other than the Cartesian is usually used (polar coordinates (r, θ), for example), in order to represent closed contours. An example of the representation of such an interface for a 3D surface is given in Figure 1.7.

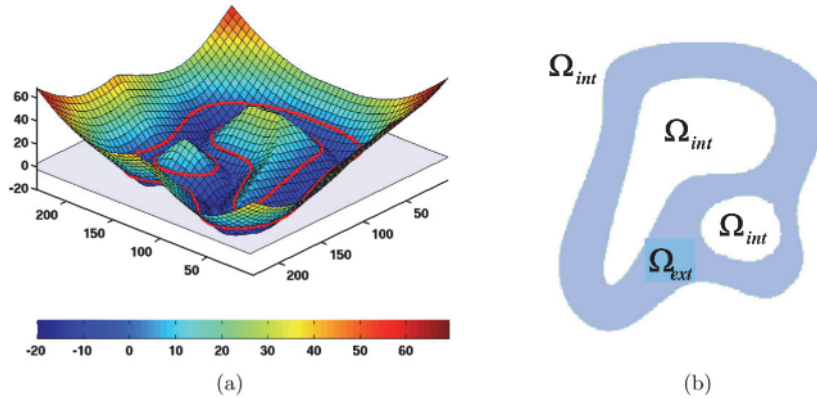

Figure 1.6. *Level sets represented as a signed distance map on a domain* Ω*. a) The implicit function* $\phi(\mathbf{p})$*. b) The inner* (Ω_{int}) *and outer* (Ω_{ext}) *domains defined by the implicit function. For a color version of this figure, see www.iste.co.uk/clarysse/cardiac.zip*

As seen above, implicit representation allows the representation of shapes with complex topology by addressing the problem in a space comprising an additional spatial dimension. At the implementation level, this implies a significant increase of the necessary memory resources as well as computation time. However, the explicit form of an interface reduces the dimensionality of the representation, which allows computation time to be significantly smaller but also the topology of segmented shapes to be constrained [BAR 12, DUA 10, VAL 06].

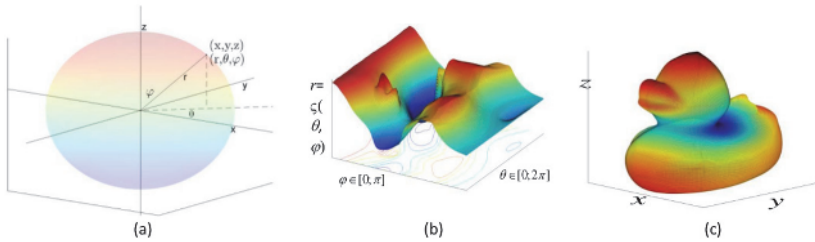

Figure 1.7. *Representation of a 3D surface using an explicit function defined on a spherical coordinate system. a) Correspondence between Cartesian and spherical coordinates. b) Explicit function represented in spherical coordinates. c) Explicit function represented in Cartesian coordinates. For a color version of this figure, see www.iste.co.uk/clarysse/cardiac.zip*

1.5.2. *Energy functional*

1.5.2.1. *General expression*

In this section, we only consider the energy functional that allows connecting the active contour to the image properties (associated with the data such as the gradient, the regional statistics differences, etc.) and, in some cases, ensuring that a smooth contour is obtained.

1.5.2.1.1. Parametric form

Through the use of the parametric representation of the interface, a general expression of this energy functional in 2D can be written as follows [JEH 03]:

$$E(\Gamma) = \int_{\Gamma} K^c(\mathbf{p})ds + \int_{\Omega_{int}} K^{int}(\mathbf{p})d\mathbf{p} + \int_{\Omega_{ext}} K^{ext}(\mathbf{p})d\mathbf{p} \quad [1.14]$$

where $d\mathbf{p} = dxdy$ is defined and ds corresponds to the parametrization of the arc length.

In this expression, the first term is a contour integral involving K^c which corresponds to a contour descriptor of the object to be detected. Thus, this descriptor is frequently based upon the gradient of the image. The last two integrals of $E(\Gamma)$ correspond, however, to region terms, and involve a descriptor of the properties of the inner region K^{int} and of the outer region K^{ext} more often based on the statistical characteristics of the image. Strictly, the dependence of the descriptors to the region should be explicitly mentioned and denoted by $K^i(\mathbf{p}, \Omega_i)$. However, this dependence will be omitted in the following for reasons of ease of writing. Further, it should be noted that certain complex criteria do not fit in this energy formulation (notably those based on distances between probability density as in [LEC 09] where the integration is done over the intensity and not over the domain). However, the principles and methodologies of derivation developed subsequently can nonetheless be used in this context.

1.5.2.1.2. Implicit form

In a pioneering work [CHA 01], Chan and Vese describe an approach that facilitates expressing the functional directly from the implicit representation

of the active contour. By using Heaviside $H(\cdot)$ and Dirac $\delta(\cdot)$ functions, the functional is then written as follows:

$$E(\phi) = \int_{\Omega} K^{c}(\mathbf{p})\delta(\phi)\,\|\boldsymbol{\nabla}\phi\|\,d\mathbf{p} + \int_{\Omega_{int}} K^{int}(\mathbf{p})H(\phi)d\mathbf{p} + \int_{\Omega_{ext}} K^{ext}(\mathbf{p})(1-H(\phi))d\mathbf{p} \quad [1.15]$$

In this expression, it can be noted that all integrals are region integrals applied to the whole domain Ω. Moreover, it can be observed that the proposed expression could be used for interfaces of any dimensions and thus particularly to the segmentation of 3D images by a surface.

1.5.2.1.3. Explicit form

The explicit form of the functional can be obtained from the implicit form using relation [1.13]. This expression is however of little interest insofar as it does not allow us to derive an evolution equation easily discretizable in the perspective of a practical implementation. We will see in contrast in section 1.5.3.1 that it is possible to obtain an evolution equation from the implicit form if it is limited to the region terms of the functional and if the explicit interface is expressed on a basis of polynomial functions.

1.5.2.2. *Main functional models*

We present here three conventional examples of functionals and the reader can refer to the following journal articles for a more complete background [OSH 03, SUR 02, TSA 03a]. For readability reasons, we also give the corresponding evolution equations of these special cases. The general approach for obtaining an evolution equation from a given functional is described in section 1.5.3.

1.5.2.2.1. Model based on the image gradient

In an article now considered to be the origin of this type of method, Caselles *et al.* proposed an active contour enabling the detection of objects characterized by high gradients on the edges while imposing the smooth character to the solution [CAS 97]. The descriptor of the object to be detected is based on the following function:

$$g(I) = \frac{1}{1 + \|\boldsymbol{\nabla} G_{\sigma} * I\|^{\alpha}} \quad [1.16]$$

where I represents the image, G_{σ} is a Gaussian with standard deviation σ and $\alpha = 1$ or 2. Therefore, the function depends on the gradient of the image

smoothed by a Gaussian filter. This function tends towards zero for high gradients and equals 1 for a zero gradient.

The functional used does not include any region term and corresponds to the following contour descriptor:

$$K^c(s) = g\left(I(\Gamma(s))\right) \quad [1.17]$$

where s corresponds to the arc length parameter. The evolution equation in parametric form is then given by:

$$\frac{\partial \Gamma(\tau)}{\partial \tau} = (g(I)\kappa - \boldsymbol{\nabla} g(I) \cdot \mathbf{N})\,\mathbf{N} \quad [1.18]$$

where κ represents the curvature of Γ and $\mathbf{N}$ represents the interior unit norm with respect to the contour. In this expression, the term depending on the curvature controls the smoothing of the curve and the second term controls the evolution under the influence of the image gradient.

Using relationship [1.31], the implicit form of the evolution equation is given by:

$$\frac{\partial \phi(\tau)}{\partial \tau} = g(I) div\left(\frac{\nabla \phi}{|\nabla \phi|}\right) \|\boldsymbol{\nabla}\phi\| + \boldsymbol{\nabla}\phi \cdot \boldsymbol{\nabla} g(I) \quad [1.19]$$

Based on this article, other contour-based approaches have been described, using a data fitting term no longer depending directly on the gradient, but on the gradient vector flow of the image [PAR 04].

1.5.2.2.2. Model based on region characteristics

In their seminal article, Chan and Vese [CHA 01] focused on the segmentation of an object showing no sharp edges, making use of information based on the gradient difficult. The functional that they proposed to solve this problem involves terms using the characteristics of the interior (Ω_{int}) and exterior regions (Ω_{ext}) defined by the active contour. The corresponding descriptors are the following:

$$\begin{cases} K^c = \mu \\ K^{int} = \nu + \lambda_1 (I - c_{int})^2 \\ K^{ext} = \nu + \lambda_2 (I - c_{ext})^2 \end{cases} \quad [1.20]$$

where c_{int} and c_{ext} correspond to the average of the image intensities of the inner and outer regions, respectively.

The functional is defined directly on the basis of the implicit representation of the active contour, and takes the following form:

$$\begin{aligned} E(\phi) = \mu \int_{\Omega} \delta(\phi) \left\| \boldsymbol{\nabla} \phi \right\| d\mathbf{p} + \nu \int_{\Omega} H(\phi) d\mathbf{p} \\ + \lambda_1 \int_{\Omega} \left(I - c_{int} \right)^2 H(\phi) d\mathbf{p} \\ + \lambda_2 \int_{\Omega} \left(I - c_{ext} \right)^2 \left(1 - H(\phi) \right) d\mathbf{p} \end{aligned} \quad [1.21]$$

The first two terms of the functional correspond, respectively, to the length of the zero level and the area of the inner region weighted by μ and ν. Their minimization therefore makes it possible to impose a smoothness constraint on the contour. The last two terms weighted by λ_1 and λ_2 are associated with the data terms and involve the averages of the image for the inner region (c_{int}) and for the outer region (c_{ext}). The minimization of these two terms will therefore tend to separate the image into two regions of uniform intensity. The evolution equation is then given by:

$$\frac{\partial \phi(\tau)}{\partial \tau} = \left(\mu div \left(\frac{\boldsymbol{\nabla} \phi}{\left\| \boldsymbol{\nabla} \phi \right\|} \right) - \nu - \lambda_1 (I - c_{int})^2 + \lambda_2 (I - c_{ext})^2 \right) \delta_{\epsilon}(\phi) \quad [1.22]$$

It should be noted that the term resulting from the minimization of the length involves the expression $div \left(\frac{\nabla \phi}{|\nabla \phi|} \right)$, which corresponds to the convention chosen for ϕ to $-\kappa$. The term δ_{ϵ} is a modified version of the Dirac function. Figure 1.8 gives an application example of this approach to a simple simulation image, comprising two homogeneous regions, with a topology involving holes in the inner region.

Other authors have proposed to take into account the statistics of the regions to segment by explicitly modeling the probability of their gray level density and by using an approach based on maximum likelihood. In practice, if the assumption is made that the random variables are independent and identically

distributed (iid), the minimized energy corresponds to the minimization of the anti-log-likelihood which implies the following descriptors:

$$\begin{cases} K^{int} = -\log(P_{int}(I(\mathbf{p}))) \\ K^{ext} = -\log(P_{ext}(I(\mathbf{p}))) \end{cases} \quad [1.23]$$

where P_{int} and P_{ext} are the two distributions chosen to characterize the object to segment and the background. By adding the smoothing term of the contour, the functional takes the following form for an implicit representation of the active contour:

$$\begin{aligned} E(\phi) = \lambda \Bigg[& -\int_{\Omega} \log(P_{int}(I(\mathbf{p})))H(\phi)d\mathbf{p} \\ & -\int_{\Omega} \log(P_{ext}(I(\mathbf{p})))(1-H(\phi))d\mathbf{p} \Bigg] \\ & +\mu \int_{\Omega} \delta(\phi)\, \|\boldsymbol{\nabla}\phi\|\, d\mathbf{p} \end{aligned} \quad [1.24]$$

When using parametric probability densities belonging to the exponential family (for example, Gaussian, Rayleigh, etc.) and under certain conditions concerning the estimation method of the hyperparameters (see [LEC 10]), the evolution equation can be written as:

$$\frac{\partial\phi(\tau)}{\partial\tau} = \left(\mu div\left(\frac{\boldsymbol{\nabla}\phi}{\|\boldsymbol{\nabla}\phi\|}\right) - \lambda\log\left(\frac{P_{int}}{P_{ext}}\right)\right)\delta_{\epsilon}(\phi) \quad [1.25]$$

[ZHU 96] have used this approach with Gaussian distributions and [CHE 99, LEC 10] have considered the more general case of distributions in the exponential family. Other authors have extended this approach to the case of non-parametric probability density [AUB 03, HER 06, JUN 05] which makes the evolution equation more complex. At last, it should be noted that [DEL 06, MAR 06] proposed to use a minimum stochastic complexity-based approach.

1.5.2.2.3. Model based on localized region characteristics

Lankton *et al.* [LAN 08] proposed an approach allowing for segmenting inhomogeneous objects for which the terms associated with the usual data based on the gradient or on a global regional characteristic lead to erroneous segmentations. This approach puts forward the hypothesis that even if the properties of the object vary spatially across the image, they can be

considered as constants if they are observed at a sufficiently local scale. This approach involves the following descriptors:

$$\begin{cases} K^c = \mu \\ K^{int}(\mathbf{p}) = \delta(\phi(\mathbf{p})) \int \Omega \lambda_1 B(\mathbf{p}, \mathbf{q}) F_{int}(I, \phi) d\mathbf{q} \\ K^{ext}(\mathbf{p}) = \delta(\phi(\mathbf{p})) \int \Omega \lambda_2 B(\mathbf{p}, \mathbf{q}) F_{ext}(I, \phi) d\mathbf{q} \end{cases} \quad [1.26]$$

where $B(\mathbf{p}, \mathbf{q})$ corresponds to a neighborhood centered at the point $\mathbf{p}$ and of size R, F_{int} and F_{ext} are region descriptors (such as those described in [1.20]). The descriptor of contour K^c is identical to that described in b) above. The descriptors of region K^{int} and K^{ext} here onward depend on the point where they are calculated and integrate in this manner purely local information. It should be observed that other authors have also proposed approaches based on the localization of the term associated with the data, such as [BRE 06, LI 08, MIL 09].

1.5.3. *Obtaining the evolution equation*

1.5.3.1. *Euler-Lagrange equations*

1.5.3.1.1. Parametric context

The minimization of the functional amounts to cancelling the first variation of $E(\Gamma)$, namely to find Γ such as:

$$\frac{\partial E}{\partial \Gamma} = 0 \quad [1.27]$$

The variation of *E* formally corresponds to a differential equation and can be technically achieved by using the Euler-Lagrange theorem or the Gâteaux-Fréchet derivatives. Due to the parametric formulation of the contour, obtaining the variation of E involves the conversion of region integrals to contour integrals, using the Green-Riemann theorem [ZHU 96]. In any dimension, this step can turn to be formally complex. This particular aspect is discussed in the article proposed by Aubert [AUB 03].

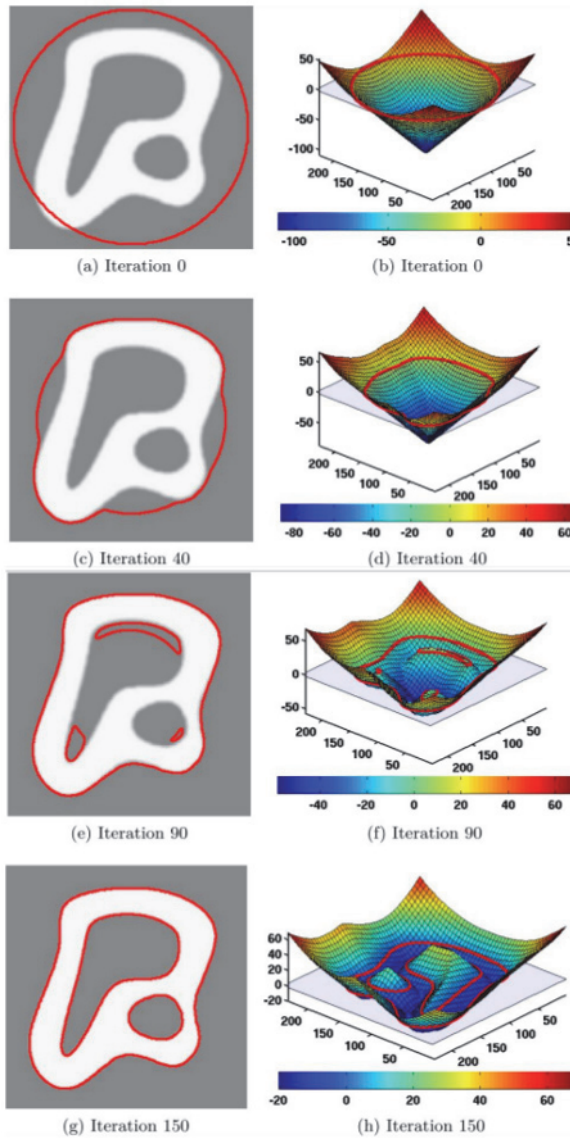

Figure 1.8. *Evolution of the implicit function for the Chan and Vese method, with the corresponding zero level in red (b, d, f, h) for synthetic images. Superposition of the zero level (red curve) on the corresponding image (a, c, e, g). For a color version of this figure, see www.iste.co.uk/clarysse/cardiac.zip*

Starting from the general expression of the functional proposed in [1.14] and restricting to the special case where the descriptors are not depending on the evolving regions and where the descriptor K^c is a constant, the Euler-Lagrange equation in two dimensions is as follows:

$$\frac{\partial E}{\partial \Gamma} = \left(-K^c\kappa - K^{int} + K^{ext}\right)\mathbf{N} \qquad [1.28]$$

where $\mathbf{N}$ is the unit norm interior to the contour and κ is the curvature. The minimization of E is then performed by a gradient descent. By introducing an artificial temporal variable τ, the evolution of the active contour equation takes the following form:

$$\frac{\partial \Gamma}{\partial \tau} = -V(\mathbf{p},\tau)\mathbf{N} \qquad [1.29]$$

where V is usually called the velocity term. The gradient descent leads to the following expression for $V(.)$:

$$V(\mathbf{p},\tau) = -K^c\kappa - K^{int} + K^{ext} \qquad [1.30]$$

Starting from this expression, it is interesting to note that the evolution of the active contour occurs only along its normal. Thus, as shown by Epstein [EPS 87], only the normal component of the velocity is necessary to control the deformation of the contour. As a matter of fact, the tangential component does not change the geometry of the contour, but only its parameterization. Furthermore, it should be noted that the use of a gradient descent leads to the fact that the minimum found in convergence is a local minimum, which consequently depends on the initial contour.

1.5.3.1.2. Implicit context

From the definition of $\phi(\mathbf{p})$ and of expression [1.29], it can be shown that the evolution equation is expressed in the following form for the implicit representation [CAS 97]:

$$\frac{\partial \phi}{\partial \tau} = V(\mathbf{p},\tau)\,\|\boldsymbol{\nabla}\phi\| \qquad [1.31]$$

As we mentioned previously, a difficulty of this type of approach in any dimension lies in the manipulation of the region terms, which can involve complex calculations to express the variation of the functional (transformation of region integrals into contour integrals). In dimensions

greater than 2, it is usually more direct and simpler to obtain the evolution equation starting from the implicit expression of the functional [1.15]. The calculation of the variation of E relative to ϕ then facilitates obtaining the associated Euler-Lagrange equation and a gradient descent provides the evolution equation that takes the following form:

$$\frac{\partial \phi}{\partial \tau} = \left(K^c div \left(\frac{\boldsymbol{\nabla} \phi}{\|\boldsymbol{\nabla} \phi\|} \right) - K^{int} + K^{ext} \right) \delta_\epsilon(\phi) \qquad [1.32]$$

It should be noted that some authors propose to amend this evolution equation by replacing the term $\delta(\phi)$ by $\|\boldsymbol{\nabla}\phi\|$ [ZHA 96]. This choice does not affect the solution upon convergence and makes the equation independent of the scale of all levels [MAR 00, TSA 03b]. Note finally that the discretization of the latter implies in practice the use of a rectified version of the Dirac function, whose examples can be found in [CHA 01].

1.5.3.1.3. Explicit context

As has already been mentioned, the principal benefit of the explicit form of the active contour consists of reducing the dimensionality of the representation, allowing the computation time to decrease and the topology of the segmented shapes to be constrained. As such, this type of representation is particularly interesting for problems in 3D, as described here. Assuming the implicit form of the functional [1.15], a relatively general form of the evolution equation can be obtained under the following conditions:

– the explicit interface is represented parametrically with the help of basis functions. Such an approach has been followed by [DUA 10, VAL 06], who used the Hermite polynomial basis functions and [BAR 12] who have implemented B-splines functions;

– a simplified form of the implicit functional [1.15] is considered, solely taking region terms into account. Actually, even in its simplest form consisting of a regularization term (that is $K^c = \text{constant}$) the calculation of the variations corresponding to the contour terms proves to be complex [VAL 06]. Moreover, the use of specific basis functions such as B-splines help to implicitly impose a smooth character on the surface.

Consider the explicit form of the interface in a coordinate system $\mathbf{p} = (u, v, w)$ in $\mathbb{R}^3$. The choice of this coordinate system depends on the type of object to segment, and most often corresponds to cylindrical, spherical or elliptical coordinates. The interface is then defined by the explicit function Ψ:

$$\Psi : \mathbb{R}^2 \to \mathbb{R},\ (u, v) \mapsto w = \Psi(u, v) \qquad [1.33]$$

It should be noted that this explicit expression is linked to the implicit form by:

$$\phi(\mathbf{p}) = \phi(u, v, w) = \Psi(u, v) - w \quad [1.34]$$

The function Ψ can be expressed as a linear combination of basis functions. We will use B-splines, here, which leads to:

$$\Psi(u, v) = \sum_{l,k \in \mathbb{R}2} c[k, l] \beta_h^d(u - k, v - l) \quad [1.35]$$

where $\beta_h^d(u, v)$ represents the symmetric uniform B-spline function of degree d, with dimension 2 and scale h and $c[k, l]$ the coefficients of the B-splines.

It is worth highlighting the purely "region" version of the functional:

$$E_{exp}(\phi) = \int_\Omega F\left(\mathbf{p}, H(\phi)\right) d\mathbf{p} \quad [1.36]$$

with:

$$F\left(\mathbf{p}, H(\phi)\right) = K^{int} H(\phi) + K^{ext}(1 - H(\phi)) \quad [1.37]$$

The interest of B-spline decomposition is that the evolution of the interface can be obtained by minimizing E_{exp} with respect to the coefficients $c[k, l]$. There is therefore a shift from a variational calculation to a simple differentiation relative to a finite set of parameters. This differentiation leads to the following expression:

$$\frac{\partial E_{exp}}{\partial c[k, l]} = \int_\Omega \frac{\partial F}{\partial \phi} \frac{\partial \phi}{\partial c[k, l]} d\mathbf{p} = \int_\Omega g(\mathbf{p}) \delta(\phi) \frac{\partial \phi}{\partial c[k, l]} d\mathbf{p} \quad [1.38]$$

with:

$$g(\mathbf{p}) = K^{int}(\mathbf{p}) - K^{ext}(\mathbf{p}) \quad [1.39]$$

By using the basic properties of the Dirac function, it can be shown for any function f the following overall result [BAR 12], which helps in shifting from the implicit expression to the explicit expression of an integral:

$$\int_\Omega f(\mathbf{p}) \delta(\phi) d\mathbf{p} = \int_\Gamma f(u, v) du dv \quad [1.40]$$

where $f(u,v)$ is the restriction of $f(\mathbf{p})$ on the interface Γ.

Applying this property, the variation of E_{exp} is thus written as:

$$\frac{\partial E_{exp}}{\partial c[k,l]} = \int_{\Gamma} g(u,v)\delta(\phi)\frac{\partial \phi}{\partial c[k,l]}dudv \qquad [1.41]$$

By using the linearity of the decomposition of ϕ [1.35] and relation [1.34], it yields:

$$\frac{\partial \phi}{\partial c[k,l]} = \beta_h^d(u-k, v-l) \qquad [1.42]$$

This last expression then leads to the final expression of the evolution of the interface:

$$\frac{\partial E_{exp}}{\partial c[k,l]} = \int_{\Gamma} g(u,v)\beta_h^d(u-k, v-l)dudv \qquad [1.43]$$

It is of interest to emphasize the benefit of this expression in terms of computation time, since it shows that the gradient of functional and therefore the evolution of the surface corresponds simply to the convolution of the term associated with the data, $g(u,v)$, with a B-spline.

1.5.3.2. *Shape gradients*

In order to calculate the evolution equation relative to the criterion $E(\Gamma)$, another alternative consists of using shape gradients and the domain derivation tools based notably on the theoretical works described in [SOK 92, DEL 01]. This method was developed in [AUB 03, JEH 03]. Here we will only recall the main elements. Let $\mathcal{U}$ be the domains set of $\mathbb{R}^2$, the optimization problem can be reconsidered by searching for an optimal partition of the image $\{\Omega_{int}, \Omega_{ext}, \Gamma\}$ where $\Omega_i \in \mathcal{U}$. The criterion is then written in the following manner as:

$$E(\{\Omega_{int}, \Omega_{ext}, \Gamma\}) = \int_{\Gamma} K^c(\mathbf{p})ds + \int_{\Omega_{int}} K^{int}(\mathbf{p}, \Omega_{int})d\mathbf{p} + \int_{\Omega_{ext}} K^{ext}(\mathbf{p}, \Omega_{ext})d\mathbf{p} \qquad [1.44]$$

The descriptors K^i are here generally considered as depending on Ω_i or not. In order to make the domain derivation understandable, we explicitly put this dependency in the descriptor. The evolution equation will be calculated from the domain derivative of the criterion E using the methodology and the tools detailed in [AUB 03]. We recall here briefly the theorems and definitions useful in this context.

1.5.3.2.1. Main definitions and theorems

The following theorem is the central theorem for the derivation of integrals of shape domains $\int_{\Omega_i} K^i(\mathbf{p}, \Omega_i)\, d\mathbf{p}$. It facilitates establishing a general relationship between the Eulerian derivative and the shape derivative.

THEOREM 1.1.– Let $\Omega_i \in \mathcal{U}$ and $\mathbf{V}$ be a vector field relative to the deformation of the domain $\Omega_i(\tau)$: $\Omega_i(\tau) = T_\tau(\mathbf{V})(\Omega_i)$ with $\tau > 0$. Under certain hypotheses on the transformation T_τ [DEL 01], the criterion $J(\Omega_i) = \int_{\Omega_i} K^i(\mathbf{p}, \Omega_i)\, d\mathbf{p}$ is differentiable, and its Eulerian derivative in the direction $\mathbf{V}$ can be expressed as follows:

$$< J'(\Omega_i), \mathbf{V} >= \int_{\Omega_i} K^i_s(\mathbf{p}, \Omega_i) d\mathbf{p} - \int_{\partial\Omega_i} K^i(\mathbf{p}, \Omega_i)(\mathbf{V} \cdot \mathbf{N})\, \mathbf{ds}$$

where K^i_s is the derivative of K^i domain. The term $\mathbf{N}$ corresponds to the unit norm interior to the contour $\partial\Omega^i$. The Eulerian derivative J in the direction $\mathbf{V}$ is defined as follows: $< J'(\Omega_i), \mathbf{V} >= \lim_{\tau\to 0} \frac{J(\Omega_i(\tau)) - J(\Omega_i)}{\tau}$. The domain derivative of K^i is defined by $K^i_s(\mathbf{p}, \Omega_i) = \lim_{\tau\to 0} \frac{K^i(\mathbf{p}, \Omega_i(\tau)) - K^i(\mathbf{p}, \Omega_i)}{\tau}$.

A proof of the previous theorem can be found in [DEL 01, SOK 92] and is also recalled in [AUB 03].

1.5.3.2.2. Methodology adopted for the calculation of the evolution equation

The following proposition provides a simple way to calculate the evolution equation of the active contour when the Eulerian derivative can be expressed as a contour integral.

PROPOSITION 1.1.– We begin from the hypothesis that the shape derivative of the criterion $J(\Omega_i)$ in the direction $\mathbf{V}$ can be written as follows:

$$< J'(\Omega_i), \mathbf{V} >= -\int_{\partial\Omega_i} v(s)(\mathbf{V} \cdot \mathbf{N}) ds$$

Based on the previous equation, the most direct choice in order to minimize $J(\Omega_i)$ consists of choosing $\mathbf{V} = \mathbf{vN}$ for the deformation of the

contour (enables the decay of energy to a minimum). We can thus derive the following evolution equation:

$$\frac{\partial \Gamma}{\partial \tau} = v(\mathbf{p}, \tau)\, \mathbf{N}$$

1.5.3.2.3. A calculation example of the evolution equation

As an example, we use here $K^i(\mathbf{p}, \Omega_i) = (I(\mathbf{p}) - c_i(\Omega_i))^2$, which corresponds to Chan and Vese's model [CHA 01]. The average c_i depends on property Ω_i and will be recalculated at each evolution of the contour. This term can also be written as a domain integral:

$$c_i(\Omega_i) = \frac{1}{|\Omega_i|} \int_{\Omega_i} I(\mathbf{p}) d\mathbf{p}$$

In this case, using Theorem 1.1, the Eulerian derivative of $J(\Omega_{int})$ can be written as follows:

$$< J'(\Omega_{int}), \mathbf{V} >= \int_{\Omega_{int}} K_s^{int}(\mathbf{p}, \Omega_{int}) d\mathbf{p} - \int_{\partial\Omega_{int}} (I(\mathbf{p}) - c_{int})^2 (\mathbf{V} \cdot \mathbf{N}) ds \quad [1.45]$$

with the domain derivative $K_s^{int} = 2 < {c_{int}}'(\Omega_{int}), \mathbf{V} > (c_{int} - I(\mathbf{p}))$. The first term of derivative [1.45] is canceled out because $< {c_{int}}'(\Omega_{int}), \mathbf{V} >$ does not depend on $\mathbf{p}$ and $\int_{\Omega_{int}} (c_{int} - I(\mathbf{p}))\, d\mathbf{p}$ is canceled. Thus, we obtain:

$$< J'(\Omega_{int}), \mathbf{V} >= - \int_{\partial\Omega_{int}} (I(\mathbf{p}) - c_{int})^2 (\mathbf{V} \cdot \mathbf{N}) ds$$

Then, we can calculate the velocity of the contour using proposition 1.1 and taking into account the fact that the inner norm of $\partial\Omega_{out}$ is the inverse of $\mathbf{N}$. It then yields:

$$\frac{\partial \Gamma}{\partial \tau} = \left[(I - c_{int})^2 - (I - c_{out})^2 + K^c \kappa - (\nabla K^c \cdot \mathbf{N}) \right] \mathbf{N}$$

The derivative of the contour term can be obtained directly using the theorems resulting from the domain optimization [DEL 01]; the term calculated by Caselles *et al.* [CAS 97] is then found again.

The advantage of this derivation is that it allows explicitly taking into account the dependence of the descriptors in the region by facilitating the

derivation in this case. Thus, in the case of more complex descriptors, the term comprising the derivative of domain K_s^i may not be null and give rise to additional terms in the equation of evolution (see [JEH 03] for more details). In the case of more complex descriptors, numerous works have also benefited from domain derivation tools to calculate the evolution equation. These include the case of probability density (parametric or non-parametric) functions that have been studied by various authors [HER 06, LEC 10]. The domain derivation tools have also been used to introduce descriptors based on Legendre moments [FOU 06].

1.5.4. *Level set digital implementation*

The implementation of the evolution equation is equivalent to solving a time-dependent differential equation. The vast majority of implementations make use of finite difference techniques. This method was initially developed by Osher and Sethian [OSH 88, OSH 02] to ensure the convergence of the algorithm towards unique and oscillatory solutions. We present here the essential points.

It may be noted, however, that some authors have recently proposed to resolve this PDE by using a continuous parametric representation of the level set. Thus, Gelas *et al.* use a collocation method and a representation by radial basis functions (RBF) [GEL 07]. Bernard *et al.* propose to use a representation with B-spline functions directly in the functional, which leads to a linear filtering-based formulation [BER 09].

A common problem that comes across involving the practical implementation of the previously described scheme is as follows: during its evolution, the level set tends to develop very flat areas or in contrast very steep fronts [MAL 95, OSH 02], which can lead to problems in terms of numerical estimation of the partial derivatives and convergence speed. The strategy commonly used to solve this problem is as follows. The level set is initialized as the signed distance function to the contour. It should be observed that such a choice leads to the fact that the gradient module of ϕ is constant, namely that $\|\boldsymbol{\nabla}\phi(\mathbf{p})\| = 1, \forall \mathbf{p} \in \Omega$.

During its evolution, the level set is periodically reinitialized in order to preserve its form of distance map. One immediate way to implement this strategy is to extract the contour points (current zero level) and recalculate distance map properties. However, this method is very costly in terms of computation time. Thus, the most commonly implemented method consists of taking advantage of the property of the distance map gradient and applying

periodically to the contour the following auxiliary evolution equation [PEN 99, SUS 99]:

$$\frac{\partial \phi(\mathbf{p},\tau)}{\partial \tau} = sign\left(\phi_0(\mathbf{p},\tau)\right)\left(1 - \|\boldsymbol{\nabla}\phi(\mathbf{p},\tau)\|\right) \quad [1.46]$$

where ϕ_0 is the function to reinitialize, $sign(\cdot)$ is the sign function.

However if ϕ_0 is not regular, the zero level corresponding to the implicit function obtained from [1.46] may be offset relative to that of the original function. To remedy this problem, Li *et al.* proposed [LI 05] to add a new term to the functional energy [1.21]:

$$E_{reg} = \int_{\Omega} \frac{1}{2}\left(\|\boldsymbol{\nabla}\phi(\mathbf{p},\tau)\| - 1\right)^2 d\mathbf{p} \quad [1.47]$$

This regularization term penalizes the level set if it moves away from a distance map. This method allows the characteristics of the level sets to be maintained as a distance map signed without needing explicit reinitialization.

In order to reduce the computation time, it should be finally pointed out that most implementations do not perform the calculations on the whole domain corresponding to the image, but in a narrow band surrounding the interface [MAL 95]. Unfortunately, this aspect of the implementation makes it more sensitive to the initialization algorithm.

1.6. Integration of *a priori* constraints in the formalism of variational contours

As mentioned at the beginning of the chapter, due to imperfections presented by images, performing a segmentation by using only the characteristics of the region or the contour proves in most cases difficult, if not impossible. These problems may be due to various factors such as significant noise, defects in contrast or occlusions related to limitations of the acquisition (see, for example, Figure 1.9). This problem can be generally managed by introducing *a priori* knowledge, relating to the shape of the object to be detected or its motion when it comes to image sequence. In this section, we describe the formulation of such *a priori* in the context of active contours.

1.6.1. *Shape a priori*

1.6.1.1. *Shape models*

Geometric models provide an approximation of the shape of the object to be detected using analytic expressions, most often depending on a low number of parameters. The adaptation of the shape to the object during the segmentation process is usually performed according to the principle of least squares. The shapes that have been used for this purpose are generally quadrics or their generalization, such as ellipses [ALE 11], hyperbolas [HAM 10], superellipses [GON 04, SAR 08] and hyperquadrics [DIE 12]. The advantage of this approach is that it requires no learning phase, which can be long and which can be moreover dependent on the acquisition plane orientation in 2D imaging. Furthermore, this type of shape does not require any alignment phase, insofar as the pose (position, orientation and scale) of the shape is an integral part of the model parameters. *A contrario*, this approach lacks generality in the sense where it assumes that the shape of the object to represent be simple enough to be approximated by an analytical form.

1.6.1.2. *Shape training*

The construction of a shape *a priori* through training assumes that a representative set of the shapes of the object to detect is available. Many modes of representation have been proposed for these shapes, such as a parametric curve [CHE 02, CHE 07], an implicit function defined as the signed distance at the interface [BRE 06, CHA 05, LEV 00] or a binary mask [FOU 06, LYN 06, ROU 02]. It is worth pointing out that a realignment phase must be applied to these forms in order to remove the variations simply due to differences in pose. This phase can be complex and it may be useful to consult [ZHA 04] for more details on re-alignment techniques.

Representation of variations in shapes originating from the training set is most often performed using a PCA, as is the case in works done in [BRE 06, CHA 05, COO 01, CRE 06a, LEV 00, TSA 03a]. Shape variations are thus synthesized through an average shape and the main modes of variation determined by the PCA. It should be noted that Foulonneau *et al.* have proposed an alternative approach based on Legendre moments, which exhibits the advantage of being invariant by affine transformation, and therefore can avoid the realignment phase [FOU 06].

1.6.1.3. *Shape constraint integration in a variational formulation*

The first approaches to integrate shape constraints in an active contour-based segmentation correspond to the ASM mentioned above [COO 95], and

to the similar approach described by Leventon *et al.* [LEV 00] for level sets. These approaches use an *a priori* described through PCA. In both cases, these approaches are not variational however, in the sense that the shape constraint is integrated directly in the evolution terms of the active contour.

A contrario, Tsai *et al.* have suggested an approach based on a shape *a priori* represented via a PCA, but expressed following a variational approach. In this approach, a shape is represented according to the set of parameters $\{\alpha, \mathbf{v_p}\}$, where α corresponds to the coordinates of the shape in the shape space derived from the PCA and $\mathbf{v_p}$ corresponds to the pose (translation, rotation and scale) of the shape. Constrained segmentation is then performed by minimizing a functional associated with the data directly in the parameter space $\{\alpha, \mathbf{v_p}\}$, which is therefore equivalent to implicitly imposing the constraint shape, according to an approach philosophically close to ASMs.

Other approaches explicitly express the constraint. In this case, the integration of the shape constraint in a variational approach implies the definition of an energy term that enables the assessment of a distance between the current active contour (that is at iteration i) and the shape *a priori*. In practice, this term is usually added, via a possible weighting, to the data attachment terms described in [1.14] or [1.15]. The first terms proposed in this framework [CRE 03a, CRE 06a, PAR 02, ROU 02, ROU 04] are most often based on the difference of the implicit functions representing the active contour $\phi(\mathbf{p})$ and the shape *a priori* $\Psi(\mathbf{p})$:

$$E_{CF}(\phi, \Psi) = \int_{\Omega} \left(\phi(\mathbf{p}) - \Psi(\mathbf{p})\right)^2 d\mathbf{p} \qquad [1.48]$$

In this equation, the implicit functions are the distance functions relative to the zero level of the level set. The evolution of the active contour is usually performed for each iteration by alternating minimization: full energy is initially minimized depending on ϕ keeping Ψ constant, then the *a priori* is updated by setting ϕ and by evolving Ψ. The characteristics of this evolution depend on the type of representation of the *a priori*: for a geometric *a priori*, the parameters defining the shape will be the ones updated. In the case of an *a priori* obtained by training, the evolution will include an update of the pose parameters, usually obtained by minimizing equation [1.48] based on these parameters (that is, rotation, translation and scaling) and keeping ϕ constant.

If equation [1.48] has the merit of being simple, it does present however a number of drawbacks. As this term depends on the square of the difference between ϕ and Ψ, the property of the distance function of these

representations must be preserved during iterations such that $E_{CF}(\phi, \Psi)$ still makes sense, which implies a systematic reinitialization of these functions throughout the definition domain Ω. Moreover, this formulation restricts the type of *a priori* it is possible to use: as a matter of fact, the result of a PCA on a set of implicit functions does not generally lead to a distance function. The same problem arises in the case of a geometric *a priori* where the expression of the shape most often corresponds to an algebraic distance. As shown in [SAM 82] and [MAT 06], the algebraic distance cannot actually be regarded as a valid approximation of the Euclidean distance in the immediate vicinity of the zero level of the level set.

Consequently, [CHA 05] have proposed a new definition of energy, according to the following expression:

$$E_{CF}(\phi, \Psi) = \int_{\Omega} \left(H(\phi(\mathbf{p})) - H(\Psi(\mathbf{p}))\right)^2 d\mathbf{p} \qquad [1.49]$$

where H is the Heaviside step function. This expression uses the indicator function of ϕ and Ψ, and thus makes the energy independent of the shape of these implicit functions.

Another expression was defined by Chen *et al.* [CHE 02], based on the distance of each point of the active contours (that is the zero level of ϕ) to the *a priori*. The energy that is derived is as follows:

$$E_{CF}(\phi, \Psi) = \int_{\Omega} \delta(\phi(\mathbf{p}))\Psi^2(\mathbf{p}) \, \|\boldsymbol{\nabla}\phi(\mathbf{p})\| \, d\mathbf{p} \qquad [1.50]$$

This expression can be interpreted as a search for a geodesic in a Riemannian space deriving from the *a priori*, namely $\Psi^2(\mathbf{p})$. The interest of this expression lies in the fact that the two implicit functions ϕ and Ψ are not being directly compared: thus, Ψ can be chosen as any implicit function, which consequently eliminates the constraints on the representation of the *a priori* identified for equation [1.48]. This energy has been so used by [ALE 11, BRE 06, CHE 02, DIE 12] and an example of its use is given in Figure 1.9.

1.6.2. *Motion a priori*

Processing image sequences offers the possibility to take advantage of the motion of the structure to be detected in order to improve and accelerate

segmentation. If certain approaches are intended to use motion as information to detect the structure of interest, others incorporate it in the form of an additional constraint. We will show a more particular preference for this last type of method.

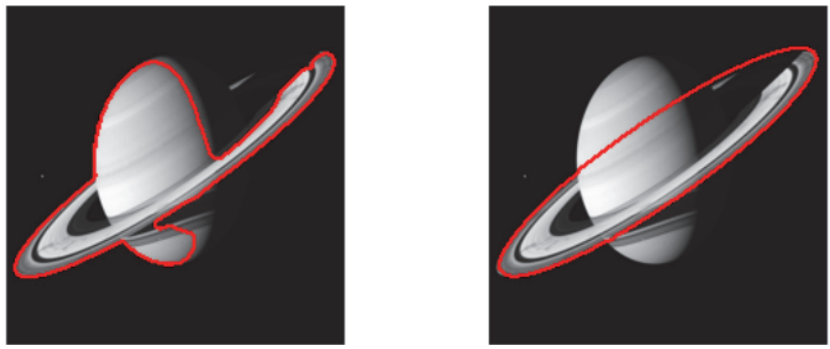

Figure 1.9. *Comparison of the segmentation of an object involving occlusion (Saturn's rings): a) without shape constraint and b) with the application of a shape constraint that allows avoiding occlusion and detecting the rings. The shape constraint is geometric here and corresponds to an ellipse. It is applied according to the approach corresponding to equation [1.50] and data fitting is a simple term of local difference of average intensity [ALE 11]. For a color version of this figure, see www.iste.co.uk/clarysse/cardiac.zip*

1.6.2.1. *Motion used as detection information*

A first approach consists of using motion, estimated jointly with the segmentation or before segmentation, as information to detect the structure, in the same way as the information derived from the intensity of the images that we have discussed in section 1.5.2.2. Similarly to the image information, such an approach therefore implies that the motion of the object presents homogeneity properties that help separate it from other structures present in the sequence. The works described in [BRO 04, BRO 06, CRE 03b, CRE 05, EHR 08, PAR 05b] follow this approach by achieving in a joint fashion the segmentation and the motion estimation. Another application of this approach can be found in [HER 04, HER 06, PAP 00, UNA 05], applied this time to image sequences where motion is estimated *a priori*, namely before the proper segmentation phase.

1.6.2.2. *Motion used as a constraint*

The usage of motion in a segmentation framework gave rise to a vast literature, involving approaches often dependent on the type of motion being considered and therefore on the application considered. It is therefore impossible to detail exhaustively or even to summarize all of the approaches in this section. We will therefore be limited here to a brief description of the techniques integrated into an active contour-based approach.

Within this framework, the majority of approaches involving the use of motion information as a constraint rely on a generalization of the technique consisting of modeling the space of eligible shapes via a PCA. In its simplest form, this approach is equivalent to considering shape variations due to motion on the same level as variations due to the inter-individual variability observed in the case of static image segmentation. However, such an approach becomes impractical when motion causes too significant shape variations: in this case the PCA must be a function of time, which leads to an *a priori* with a dynamic shape.

1.6.2.2.1. ASM and AAM technique generalization

The approach proposed by Bosch *et al.* [BOS 02] consists of a generalization of the AAMs and is applied in ultrasound echocardiographic imaging. The construction of the model is carried out with the set of images from the training sequences. Similarly, the segmentation phase is applied to the whole cardiac sequence to process. Casero *et al.* [CAS 08] offer, for their part, a generalization of ASMs where the temporal dimension is explicitly taken into account using a kernel-based PCA, which corresponds to a nonlinear form of the PCA. In a recent study, Leung *et al.* propose to define the constraint by applying a PCA to motion itself [LEU 11]. This PCA is performed by approximating the inter-frame motion by means of an affine transformation. This motion model is then used to constrain a motion estimation based on the conventional optical flow. The knowledge of the initial contour in the sequence and of motion thus estimated makes it possible to segment all the images in the sequence.

1.6.2.2.2. State model prediction

In combination or independently of these dynamic PCA, a number of approaches focus on predicting and/or constraining the segmentation at a given time by applying a motion model to the segmentations achieved in the preceding instants. In the field of medical imaging and in particular in that of cardiac and pulmonary imaging, this approach is confronted with the fact that explicit motion modeling is not available. As a result, motion is often

exploited in the form of a discrete field of velocity/motion obtained via a numerical estimation (such as optical flow-based for example) applied to the data to be processed. When modeling becomes necessary, it is frequently performed in the form of a state system, which presents several advantages. On the one hand, the parameters of the model can be estimated from a set of training sequences and/or directly from the sequence to process and on the other hand, prediction/filtering approaches such as Kalman filter-based can then be deployed.

Malassiotis was one of the first to follow this approach [MAL 99]. In the proposed approach, a shape model is built via a PCA applied on the fly to the data to be processed: the contour detected in an image is therefore used to update the PCA and process the following image. A Kalman filter is implemented to merge the information provided by a "snake"-based active contour in the current image (measurement step of the filter) and the application of a simple dynamic system of order 0 to the parameters of the PCA provides the prediction step. In the same spirit, Jacob *et al.* also use an approach based on PCA and Kalman filtering [JAC 99]. In these works, the measurement step of the Kalman filter corresponds to the evaluation of the image gradient or to the phase operator developed in [MUL 00]. The dynamic aspect is taken into account by expressing the evolution of the parameters of the shape model using an autoregressive model of order 2, whose parameters are estimated over a training sequence. The implementation of this dynamic model then allows the prediction of the filter stage to be achieved. Comaniciu *et al.* have, for their part, formulated the segmentation of a sequence as an information fusion problem, based on a Kalman filter and a particular form of the PCA, named strongly adapted PCA (SA-PCA) [COM 04]. For a sequence to be processed, the latter consists of updating the PCA with the initial contour of the sequence, in order to take into account the shape variations that might not be reflected by the standard PCA. In this approach, an initial contour is provided then propagated taking into account both the estimated motion [COM 03] and the shape model. The robustness of the approach lies in the fact that the fusion stage of the Kalman filter takes into account three sources of uncertainties related to the dynamics of the associated state system, to the shape model provided by the PCA and the measurement of the motion field. In this approach, a dynamic system of order 0 is used. Finally, it is worth noting the approach proposed in [PAP 08], which is based on purely variational modeling combined with a dynamic model applied not only to the contour but also to the motion field to follow.

1.6.2.2.3. Constraint application in a variational approach

Other authors have addressed image sequence segmentation by expressing motion constraint in a variational framework. There again, the constraint expression often passes through a modeling phase via a PCA.

Thus, Kohlberger *et al.* address three-dimensional (3D) image sequences segmentation by performing a PCA in 4D and by using an implicit representation of the considered surfaces [KOH 06]. Segmentation is then achieved by minimizing energy with a conventional data fitting term and a constraint term of the form given in [1.48]. As in [TSA 03a], this minimization is performed in the parameters space of the PCA. In the same vein, the technique described in [PAR 05a] is specifically adapted for cardiac imaging. It also relies on a PCA achieved on an implicit representation of contours. This PCA is applied to two particular instants, corresponding to the systolic and diastolic ventricular contours. The dynamic aspect of the problem is then taken into account by building a model corresponding to a linear combination of the systolic and diastolic models. After a model updating phase, segmentation is then carried out for each image in the sequence by minimizing the energy describing the distance of the model to the data in the space defined by the PCA. For their part, Cremers *et al.* develop an approach that is defined in the same spirit as Jacob *et al.* [JAC 99] but is formalized in a variational framework and uses an implicit representation [CRE 06b]. A PCA is performed on each image of a set of training sequences and modeling the dynamics of the *a priori* thus obtained is achieved by representing the evolution of the parameters of the PCA through an autoregressive model of order 2. The segmentation of an image of the sequence to process is then performed by minimizing the energy consisting of a data-fitting term under the hypothesis of a Gaussian distribution of the gray levels and of a constraint term calculated by applying the autoregressive model to the parameters of the PCA representation of the previous contours.

A number of other works based on variational formulations do not take advantage of modeling with PCA, but express very specific constraints to the intended application.

In cardiopulmonary imaging by MRI, Zhang and Pless use a manifold training technique to integrate a motion *a priori* in a segmentation approach with a level set ϕ [ZHA 05]. Manifold learning is applied to MRI sequences before segmentation in order to represent the temporal variations of the image according to two degrees of freedom corresponding to the phases of cardiac motion, u, and the phases of the respiratory motion ν. This training indicates that when considering a trajectory only along the respiratory phases, the heart

motion corresponds to a global translation of vector $V = (\omega_x, \omega_y)$, while a trajectory along the cardiac phases is close to a dilation or a pure expansion, which can simply be expressed in implicit form such as the addition of a constant ω_u at all levels ϕ. This observation has led the authors to introduce an additional energy term, $E_{CM}(\phi)$, making it possible to constrain the variation of the level set according to the two dimension u and ν of the manifold. This term is then of the form:

$$E_{CM}(\phi) = \eta_1 \int_\Omega \left(\frac{\partial \phi}{\partial x}\omega_x + \frac{\partial \phi}{\partial y}\omega_y + \frac{\partial \phi}{\partial \nu} \right)^2 d\mathbf{p} + \eta_2 \int_\Omega \left(\omega_u - \frac{\partial \phi}{\partial u} \right)^2 d\mathbf{p} \quad [1.51]$$

with $\phi : \mathbb{R}^4 \to \mathbb{R}$, $(x, y, u, \nu) \mapsto \phi(x, y, u, \nu)$ where x and y correspond to the spatial coordinates. In this approach, the authors use the region data fitting term defined in [CHA 01] and described in section 1.5.2.2.

Zhu *et al.* [ZHU 07, ZHU 10] propose to use the incompressibility of the myocardium to constrain the segmentation of 3D echocardiographic image sequences. In this approach, the myocardium is represented using two implicit surfaces corresponding to the endocardium and the epicardium ϕ_i and ϕ_o, which allows the myocardial volume to be expressed in the form:

$$V = \int_\Omega \left(H\left(\phi_o(\mathbf{p})\right) - H\left(\phi_i(\mathbf{p})\right) \right) d\mathbf{p} \quad [1.52]$$

The problem is then formalized in a Bayesian framework where the data fitting term makes the assumption of a Rayleigh distribution and where the variation of the myocardial volume around the mean is modeled through a Gaussian distribution of the form:

$$p(V) = \frac{1}{\sqrt{2\pi}} exp\left(-\frac{(V - V_o)^2}{2\sigma^2} \right) \quad [1.53]$$

where V_o and σ represent, respectively, the mean and the standard deviation of the volume.

In the same spirit as in [ZHU 10], Lynch *et al.* have introduced a global constraint relating to the evolution of the ventricular volume in the segmentation of 3D cardiac MRI images by level sets [LYN 08]. This constraint makes it possible to express the evolution of the level set in a parametric form whose parameters are estimated from a coarse

pre-segmentation of the ventricle. It should be pointed out, however, that this approach is not variational since the constraint is introduced directly into the evolution term of the level set.

1.7. Implementation examples in cardiac imaging

We present in this section the implementation of variational active contour methods in cardiac imaging, describing the choices carried out and locating them relative to the previous general sections. Such an approach implies a significant restriction of the number of examples that can be processed. Accordingly, we are focused here on two examples of active contours, applied to the segmentation of cardiac ultrasound images in 2D and 3D ultrasound echography. The reader eager to obtain more information about heart and/or chest segmentation in other modalities can refer to journal articles concerning the segmentation of heart images [KAN 12, MIT 02], and more specifically [LEU 10, NOB 06] in ultrasound heart imaging, [PET 11] in cardiac MRI and [LO 10, SLU 06, VAN 12] for the segmentation of CT lung structures.

1.7.1. *Echographic imaging: choice of the data fitting term*

As we have mentioned, the choice of the data fitting term depends on relevant information that it is possible to extract from the image with the aim to separate the structures to segment, and thus, it depends on the modality considered. In terms of segmentation, ultrasound images present a number of well-known specificities: inhomogeneous contrast, possible presence of shadow cones, granularity in homogeneous tissue (speckle). Figure 1.10 shows a few examples of these specificities.

Among these characteristics, the main one is the presence of *speckle*, inevitable as intrinsically linked to the formation process of the ultrasound image in biological tissues. As such, the use of conventional differential terms such as gradients proves difficult and many authors have suggested building data fitting terms based on the statistics of the ultrasound images by using functionals originated in the explicit modeling of speckle statistics of the form given in [1.24]. According to the type of tissue or to the acquisition conditions, some authors have proposed a Gaussian [LIN 03], a generalized Gaussian [BER 07], a Rayleigh [DYD 06, SAR 05], a gamma [TAO 07], Nagakami's distribution [ZHU 10]. Other authors make use of statistical global parameters, such as the regional dispersion of gray levels relative to the average, as we have already seen with Chan and Vese [CHA 01] with the

energy given in [1.15] or the difference of the average gray levels according to the form proposed by Yezzi [YEZ 02]:

$$E(\phi) = -\left(c_{int} - c_{ext}\right)^2 \qquad [1.54]$$

where c_{int} and c_{ext} are the averages of the regions intensities corresponding respectively to the inner and outer regions of the contour.

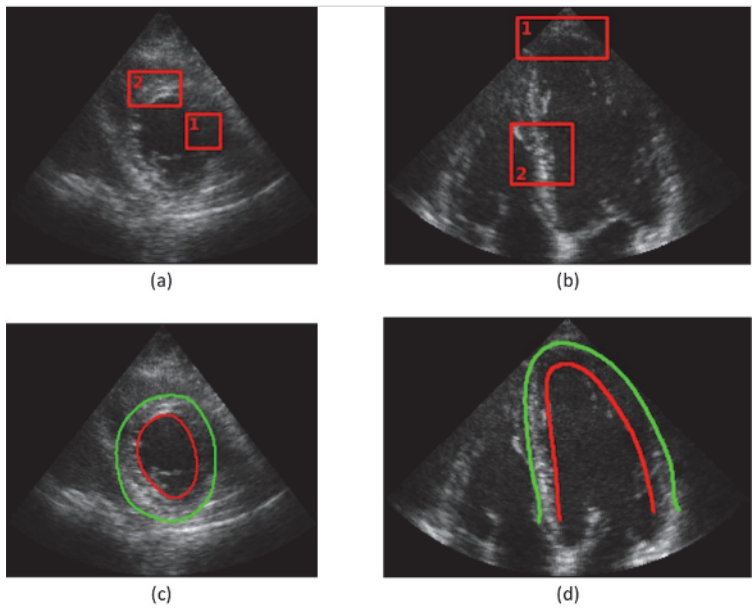

Figure 1.10. *Example of inhomogeneities in ultrasound heart imaging with a short-axis a) and apical four-chamber b) parasternal views. Images c) and d) provide for these same images the contours of the epicardium (in green) and the endocardium (in red) traced by a cardiologist. In (a), the inhomogeneity of the image causes a drop in contrast in region 1 relative to region 2. In (b), the apical region (region 1) is fuzzy and present a lower contrast than the septum region (region 2) due to the fact that the apex is located in the field near the probe. For a color version of this figure, see www.iste.co.uk/clarysse/cardiac.zip*

As we have mentioned above, diffraction, attenuation phenomena as well as the variation in orientation of the ultrasonic beam relative to the diffusers make the properties of the image inhomogeneous. That is why the use of global statistics, estimated over the whole image, is generally poorly adapted in order to obtain a satisfactory segmentation. Thus, a number of authors [ALE 11,

ALE 09, BEL 11, DIE 12] have suggested to locate these statistics using the formulation described in [LAN 08] for implicit active contours, and given in previous sections in [1.26].

1.7.2. *Example of 3D echocardiography image segmentation*

One of the major interests of ultrasound imaging is its ability to acquire data in real-time, which makes it particularly well suited for the examination of dynamic phenomena such as the cardiac cycle. The segmentation methods developed for this type of data are most often committed to preserve this dynamic aspect by providing results with computation times compatible with the flow of 3D images [BAR 12, DUA 08, ORD 08, ZHU 10].

The example presented here is taken from the works described at the methodological level in [BAR 12] and evaluated at the level of the medical application in [BAR 13a, BAR 13b]. The representation of the active surface (surface and not contour, the problem being 3D) is an explicit representation of the type presented in [1.33], using spherical coordinates and modeled by B-splines. In the context of the segmentation of 3D echocardiographic data, this expression has two points of interest. First, the restriction of the solution to functions defined on a B-spline basis make it possible to introduce implicit *a priori* smoothing in the segmentation, smoothing controlled by the degree and the scale of the B-splines being used. It thus avoids introducing the usual smoothness term associated with the curvature (see [1.22]) and thereby improves computation time. In the second place, as has been demonstrated in [1.43], the evolution of the surface simply corresponds to a B-spline convolution, which also helps there to improve in computation time and thus to develop a fast algorithm to handle sequences of 3D images.

The data fitting term used in this approach [BAR 13a] is inspired by the term due to Yezzi and previously mentioned [1.54]. This term is symmetric in the sense where, because of the square, it will be sensitive to a difference in average, whether positive or negative. The effective term used is simply the following:

$$E(\phi) = c_{int} - c_{ext} \qquad [1.55]$$

It facilitates to take advantage of the fact that in echocardiography, the inner region of the ventricle is darker than the outer: as a matter of fact, it is positive otherwise and then causes an increase of energy, which will be therefore penalized during the minimization of functional. Finally, it should

be observed that this fitting term is applied in a local context according to the approach of [LAN 08], described in section 1.5.2.2. The function $g(x, y)$ governing the evolution of the active surface (see [1.43]) is then given by:

$$g(x,y) = \frac{1}{A_{int}} \left(I(x,y) - c_{int}\right) - \frac{1}{A_{ext}} \left(I(x,y) - c_{ext}\right) \qquad [1.56]$$

where A_{int} and A_{ext} are the area of the regions inside and outside the surface used to locally estimate the averages c_{int} and c_{ext}.

Figure 1.11 provides an example of results obtained on a cardiac volume. The approach has been evaluated for the measurement of the left ventricular volume in [BAR 13a]. In this study, the initialization phase of the active surface, which is difficult and time-consuming in 3D, is performed using an automatic procedure. The study was conducted with a set of 24 cardiac volumes acquired at the end of the systole and of the diastole on healthy and pathological subjects and the achieved volumes have been compared with those originated from the segmentation provided by three experts. It has allowed us to obtain correlation coefficients higher than 0.97. Computation times are of the order of the second for the initialization phase and segmentation itself corresponds to computation times smaller than 60 ms.

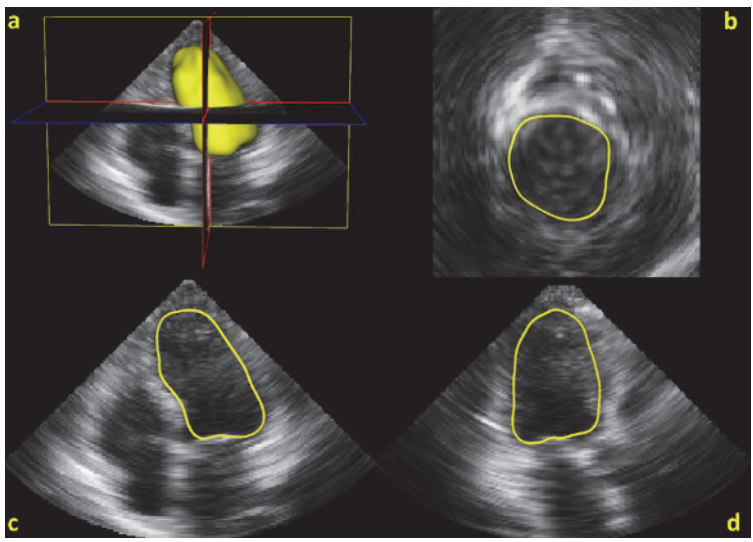

Figure 1.11. *Segmentation results with end-diastolic cardiac 3D data: a) visualization of three sliceal views and of the segmented volume; minor-axis b) and major-axis c)–d) views, presented with the intersection of the segmented volume. For a color version of this figure, see www.iste.co.uk/clarysse/cardiac.zip*

1.7.3. *Example of 2D echocardiography image segmentation*

The segmentation of 2D cardiac echography images raises specific issues: the shape of the heart is highly variable depending on the chosen observation plane and the limited acquisition angle can lead to the fact that the cardiac structures are only partially visible. The example presented here is based on the works described in [DIE 12] and helps to detail the implementation of data-fitting terms, of shape constraints and motion.

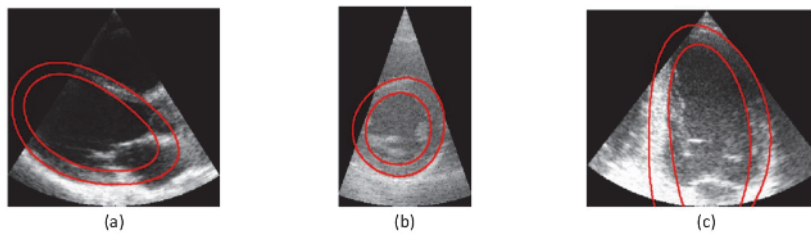

Figure 1.12. *Approximation examples of the shape of the myocardium by a pair of hyperquadrics in major-axis parasternal a), small-axis parasternal b) and apical 2 chamber c) views. For a color version of this figure, see www.iste.co.uk/clarysse/cardiac.zip*

The representation of the active contour chosen in this work is implicit. The data-fitting term is based on the conventional mean-deviation term [CHA 01], realized with the local estimation [LAN 08], seen in section 1.5.2.2.

This type of term is however not able to compensate for inhomogeneities leading to the near-disappearance of the contrast already mentioned. This problem is all the more reinforced in 2D imaging by the fact that cardiac structures may only be partially visible. Moreover, segmentation must avoid including papillary muscles that may appear within the image field during the cardiac cycle. This observation has led to the introduction of a geometric shape *a priori* based on hyperquadrics [DIE 12]. This constraint is introduced by using the implicit representation of the hyperquadrics and the functional measuring the distance between the active contour and the *a priori* according to the formulation given in [1.50]. This choice presents several interests. At the application level, the implicit representation chosen for this *a priori* allows both the outline of the endocardium and the epicardium to be modeled by a couple of hyperquadrics. Moreover, the flexibility of this type of shape enables this modeling to be achieved for the four echocardiographic views commonly used in clinical routine (short-axis parasternal, long-axis parasternal, two-chamber apical and four-chamber apical), as shown in

Figure 1.12. At the implementation level, this formulation yields the fact that the adaptation of the two hyperquadrics to a set of points simply summarizes to a least squares problem. During the direct application of the approach described above, the authors have noted that some images were driving the contours of the level set corresponding to the endocardium and the epicardium to merge. This problem has been addressed by introducing an additional constraint consisting of locally imposing a minimum thickness to the detected myocardium. On the variational level, this specific constraint is expressed as follows:

$$E_{thickness}(\phi) = \int_{\Omega} \phi\left(\mathbf{p} + R_E\mathbf{N}\right) \cdot H\left(\phi\left(\mathbf{p} + R_E\mathbf{N}\right)\right) \cdot \delta\left(\phi(\mathbf{p})\right) d\mathbf{p} \quad [1.57]$$

where $\mathbf{N}$ is the normal to the active contour at the point $\mathbf{p}$ and R_E the minimum value of the desired thickness. Figure 1.13 allows us to observe the influence of this single term on a simple segmentation (using no shape constraint).

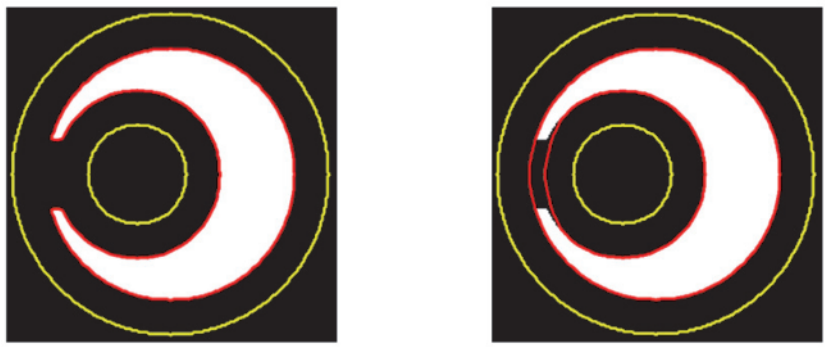

Figure 1.13. *Illustration of the local influence of the thickness constraint term on the result of the segmentation. The active contour initialization is in yellow and the final result of the segmentation is in red. The figure helps to compare the result obtained without thickness constraint a) and with thickness constraint b). For a color version of this figure, see www.iste.co.uk/clarysse/cardiac.zip*

This segmentation algorithm was in the first place evaluated on static images. The data included 80 images acquired according to the usual four echocardiographic views and coming from 20 healthy patients. The reference contours have been traced by three cardiologists for each image. The error obtained under these conditions and measured as the absolute average distance to the reference contour was equal to 1.31 mm in average and has proved close to the inter-observer variability (1.29 mm).

The approach was subsequently extended to the segmentation of temporal sequences of images [DIE 13]. This extension was carried out by introducing in the variational approach a motion constraint term, formally close to the approach described in [ZHA 05] and mentioned in section 1.6.2.2. In this approach, motion is modeled as a dense velocity field, assumed as known *a priori*. This motion has been estimated by an optical flow approach adapted to the monogenenic representation of the ultrasonic image [ALE 13a, ALE 13b]. By analogy with the constraint used in optical flow, the constraint used presupposes the conservation of the zero level of the implicit function by means of the motion. This assumption leads to the following functional:

$$E_{CM}(\phi) = \int_{\Omega} \delta(\phi(\mathbf{p})) \left(\nabla\phi(\mathbf{p}) \cdot \mathbf{V}(\mathbf{p}) + \phi_t(\mathbf{p})\right)^2 d\mathbf{p} \qquad [1.58]$$

where $\mathbf{V}(\mathbf{p})$ is the velocity field and $\phi_t(\mathbf{p})$ is the time derivative of the implicit function.

In terms of evaluation, this approach has been applied to 20 sequences representing approximately 1200 images acquired in three usual echocardiographic views with healthy patients. The reference contours have been traced by two experts. The quality of the results is reflected by the value of the error (mean absolute distance to the reference contour) which amounts to 0.90 mm on average and is significantly lower than the inter-observer variability (1.41 mm). An example of segmentation obtained for several moments in three echocardiographic views is given in Figure 1.14.

1.8. Conclusion

The segmentation of cardiac structures remains an open problem, despite several decades of methodological development. Today, however, fairly effective methods have been developed in 2D and 3D whose performance are now evaluated for example through *challenges* which have emerged in the international congresses of the field. The comparative evaluation of methods in terms of segmentation quality, speed and ease of implementation, is required to envisage a use in a clinical context. Section 1.5 offers a panorama of the different evaluation strategies and of the measures used in this area. Finally, beyond the contours, it is also important to be able to distinguish the different types of identifiable myocardial tissues, for example, in different varieties of MR images (T1-weighted imaged, delayed enhancement, etc.). Delayed enhancement MR images facilitate in particular the identification of necrosis areas. Numerous analysis methods of these images based on more or

less sophisticated image processing have been proposed to help the automated categorization of myocardial tissues [AMA 04, BEE 09, HEN 13, HSU 06b, HSU 06a, KAC 08, POS 05, VAL 11]. All these developments constitute an essential building block to deliver quantitative parameters of clinical interest (cavities volume, myocardial mass, lesion volume, ejection fraction, etc.) and to feed heart "specific patient" models which are the subject of Chapter 9.

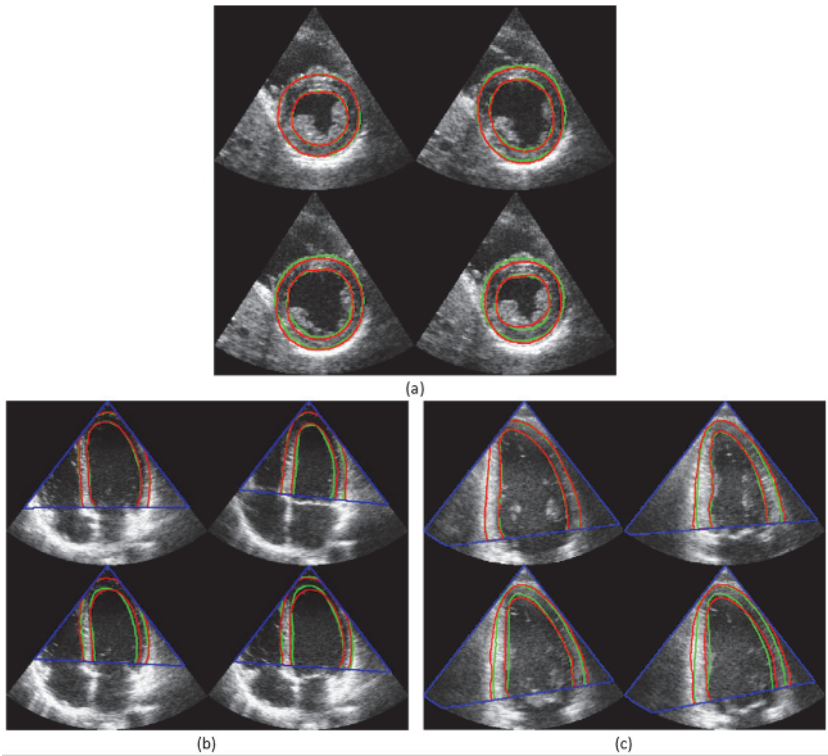

Figure 1.14. *Examples of the segmentation of 2D echocardiographic image sequences for three common views. For each example, four equidistant moments in the sequence are shown with the contours of reference in green and the result of segmentation in red. a) Short-axis parasternal view, b) apical four-chamber view, c) apical two-chamber view. For a color version of this figure, see www.iste.co.uk/clarysse/cardiac.zip*

1.9. Bibliography

[ALE 09] ALESSANDRINI M., FRIBOULET D., BASSET O. *et al.*, "Level-set segmentation of myocardium and epicardium in ultrasound images using localized Bhattacharyya distance", *IEEE International Ultrasonics Symposium*, pp. 2468–2471, 2009.

[ALE 11] ALESSANDRINI M., DIETENBECK T., BASSET O. *et al.*, "Using a geometric formulation of annular-like shape priors for constraining variational level-sets", *Pattern Recognition Letters*, vol. 32, no. 9, pp. 1240–1249, 2011.

[ALE 13a] ALESSANDRINI M., BASARAB A., LIEBGOTT H., "Myocardial motion estimation from medical images using the monogenic signal", *IEEE Transactions on Image Processing*, vol. 22, pp. 1084–1095, 2013.

[ALE 13b] ALESSANDRINI M., LIEBGOTT H., BARBOSA D. *et al.*, "Monogenic phase based optical flow computation for myocardial motion analysis in 3D echocardiography", vol. 7746, *Lecture Notes in Computer Science*, Chapter 19, pp. 159–168, Springer, Berlin-Heidelberg, 2013.

[ALL 07] ALLASSONNIÈRE S., AMIT Y., TROUVÉ A., "Towards a coherent statistical framework for dense deformable template estimation", *Journal of the Royal Statistical Society: Series B (Statistical Methodology)*, vol. 69, no. 1, pp. 3–29, 2007.

[AMA 04] AMADO L.C., GERBER B.L., GUPTA S.N. *et al.*, "Accurate and objective infarct sizing by contrast-enhanced magnetic resonance imaging in a canine myocardial infarction model", *Journal of the American College of Cardiology*, vol. 44, no. 12, pp. 2383–2389, 2004.

[AUB 03] AUBERT G., BARLAUD M., FAUGERAS O. *et al.*, "Image segmentation using active contours: calculus of variations for shape gradients?", *SIAM Journal on Applied Mathematics*, vol. 63, no. 6, pp. 2128–2154, 2003.

[AUJ 05] AUJOL J., CHAMBOLLE A., "Dual norms and image decomposition models", *International Journal of Computer Vision*, vol. 63, no. 1, pp. 85–104, 2005.

[BAR 12] BARBOSA D.C., DIETENBECK T., SCHAERER J., *et al.*, "B-Spline Explicit Active Surfaces: An efficient framework for real-time 3D region-based segmentation", *IEEE Transactions on Image Processing*, vol. 21, no. 1, pp. 241–251, 2012.

[BAR 13a] BARBOSA D.C., DIETENBECK T., HEYDE B. *et al.*, "Fast and fully automatic 3D echocardiographic segmentation using B-spline explicit active surfaces: feasibility study and validation in a clinical setting", *Ultrasound in Medicine and Biology*, vol. 39, no. 1, pp. 89–101, 2013.

[BAR 13b] BARBOSA D.C., HEYDE B., DIETENBECK T. *et al.*, "Quantification of left ventricular volume and global function using a fast fully automated segmentation tool: validation in a clinical setting", *International Journal of Cardiovascular Imaging*, vol. 29, no. 2, pp. 309–316, 2013.

[BEE 09] BEEK A., BONDARENKO O., AFSHARZADA F. *et al.*, "Quantification of late gadolinium enhanced CMR in viability assessment in chronic ischemic heart disease: a comparison to functional outcome", *Journal of Cardiovascular Magnetic Resonance*, BioMed Central, vol. 11, no. 1, pp. 1–7, 2009.

[BEL 11] BELAID A., BOUKERROUI D., MAINGOURD Y. *et al.*, "Implicit active contours for ultrasound images segmentation driven by phase information and local maximum likelihood", *IEEE International Symposium on Biomedical Imaging (ISBI)*, pp. 630–635, 2011.

[BER 07] BERNARD O., TOUIL B., GELAS A. *et al.*, "A RBF-based multiphase level set method for segmentation in echocardiography using the statistics of the radiofrequency signal", *IEEE International Conference on Image Processing (ICIP'07)*, vol. 3, pp. 157–160, 2007.

[BER 09] BERNARD O., FRIBOULET D., THÉVENAZ P. *et al.*, "Variational B-spline level-set: a linear filtering approach for fast deformable model evolution", *IEEE Transactions on Image Processing*, vol. 18, no. 6, pp. 1179–1191, 2009.

[BOS 02] BOSCH J., MITCHELL S., LELIEVELDT B. *et al.*, "Automatic segmentation of echocardiographic sequences by active appearance motion models", *IEEE Transactions on Medical Imaging*, vol. 21, no. 11, pp. 1374–1383, 2002.

[BOY 06] BOYKOV Y., KOLMOGOROV V., CREMERS D. *et al.*, "An integral solution to surface evolution PDEs via geo-cuts", *ECCV*, pp. 409–422, 2006.

[BRE 06] BRESSON X., VANDERGHEYNST P., THIRAN J.-P., "A variational model for object segmentation using boundary information and shape prior driven by the Mumford-Shah functional", *International Journal of Computer Vision*, vol. 68, no. 2, pp. 145–162, 2006.

[BRE 07] BRESSON X., ESEDOGLU S., VANDERGHEYNST P. *et al.*, "Fast global minimization of the active contour/snake model", *Journal of Mathematical Imaging and Vision*, vol. 28, pp. 151–167, 2007.

[BRO 04] BROX T., BRUHN A., PAPENBERG N. *et al.*, "High accuracy optical flow estimation based on a theory for warping", *European Conference on Computer Vision (ECCV)*, vol. 3024, pp. 25–36, 2004.

[BRO 06] BROX T., BRUHN A., WEICKERT J., "Variational motion segmentation with level sets", LEONARDIS A., BISCHOF H., PINZ A. (eds), *European Conference on Computer Vision (ECCV)*, vol. 3951, pp. 471–483, 2006.

[BRO 12] BROWN E., CHAN T., BRESSON X., "Completely convex formulation of the Chan-Vese image segmentation model", *International Journal of Computer Vision*, vol. 98, no. 1, pp. 103–121, 2012.

[CAS 93] CASELLES V., CATTE F., COLL T. *et al.*, "A geometric model for active contours", *Numerische Mathematik*, vol. 66, pp. 1–31, 1993.

[CAS 97] CASELLES V., KIMMEL R., SAPIRO G., "Geodesic active contours", *International Journal of Computer Vision*, vol. 22, no. 1, pp. 61–79, 1997.

[CAS 08] CASERO R., NOBLE J., "A novel explicit 2D+t cyclic shape model applied to echocardiography", *Medical Image Computing and Computer-Assisted Intervention (MICCAI)*, vol. 5241, pp. 527–534, 2008.

[CAS 10] CASTA C., CLARYSSE P., POUSIN J. *et al.*, "Incorporating low-level constraints for the retrieval of personalised heart models from dynamic MRI", *Statistical Atlases and Computational Models of the Heart*, vol. LNCS 6364, pp. 174–183, Springer-Verlag, Berlin-Heidelberg, 2010.

[CAS 12] CASTA C., Estimation 3D conjointe forme/structure/mouvement dans des séquences dynamiques d'images. Application à l'obtention de modèles cardiaques patients spécifiques anatomiques et fonctionnels, Thesis, INSA, Lyon, 2012.

[CHA 99] CHAN T., GOLUB G., MULET P., "A nonlinear primal-dual method for total variation-based image restoration", *SIAM Journal on Scientific Computing*, vol. 20, no. 6, pp. 1964–1977, 1999.

[CHA 01] CHAN T., VESE L., "Active contours without edges", *IEEE Transactions on Image Processing*, vol. 10, no. 2, pp. 266–277, 2001.

[CHA 04] CHAMBOLLE A., "An algorithm for total variation minimization and applications", *Journal of Mathematical Imaging and Vision*, vol. 20, nos. 1–2, pp. 89–97, 2004.

[CHA 05] CHAN T., ZHU W., "Level set based shape prior segmentation", *IEEE Conference on Computer Vision and Pattern Recognition – CVPR*, vol. 2, pp. 1164–1170, 2005.

[CHE 99] CHESNAUD C., REFREGIER P., BOULET V., "Statistical region snake-based segmentation adapted to different physical noise models", *IEEE Transactions on Pattern Analysis and Machine Intelligence*, vol. 21, no. 11, pp. 1145–1157, 1999.

[CHE 02] CHEN Y., TAGARE H.D., THIRUVENKADAM S. *et al.*, "Using prior shapes in geometric active contours in a variational framework", *International Journal of Computer Vision*, vol. 50, no. 3, pp. 315–328, 2002.

[CHE 07] CHEN Y., HUANG F., TAGARE H. *et al.*, "A coupled minimization problem for medical image segmentation with priors", *International Journal of Computer Vision*, vol. 71, no. 3, pp. 259–272, 2007.

[COH 91] COHEN L., "On active contour models and balloons", *Computer Vision, Graphics and Image Processing*, vol. 53, pp. 211–218, March 1991.

[COM 03] COMANICIU D., "Nonparametric information fusion for motion estimation", *IEEE Conference on Computer Vision and Pattern Recognition (CVPR)*, vol. 1, pp. 59–66, 2003.

[COM 04] COMANICIU D., ZHOU X., KRISHNAN S., "Robust real-time myocardial border tracking for echocardiography: an information fusion approach", *IEEE Transactions on Medical Imaging*, vol. 23, no. 7, pp. 849–860, 2004.

[COO 95] COOTES T.F., TAYLOR C.J., COOPER D.H. *et al.*, "Active shape models-their training and application", *Computer Vision and Image Understanding*, vol. 61, no. 1, pp. 38–59, 1995.

[COO 01] COOTES T.F., EDWARDS G.J., TAYLOR C.J., "Active appearance models", *IEEE Transactions on Pattern Analysis and Machine Intelligence*, vol. 23, no. 6, pp. 681–685, 2001.

[CRE 03a] CREMERS D., "A variational framework for image segmentation combining motion estimation and shape regularization", *IEEE Conference on Computer Vision and Pattern Recognition (CVPR)*, vol. 1, pp. 53–58, 2003.

[CRE 03b] CREMERS D., SOCHEN N., SCHNORR C., "Towards recognition-based variational segmentation using shape priors and dynamic labeling", *International Conference on Scale Space Theories in Computer Vision*, vol. 2695, Springer-Verlag, pp. 388–400, 2003.

[CRE 05] CREMERS D., SOATTO S., "Motion competition: a variational approach to piecewise parametric motion segmentation", *International Journal of Computer Vision*, vol. 62, no. 3, pp. 249–265, 2005.

[CRE 06a] CREMERS D., "Dynamical statistical shape priors for level set-based tracking", *IEEE Transactions on Pattern Analysis and Machine Intelligence*, vol. 28, no. 8, pp. 1262–1273, 2006.

[CRE 06b] CREMERS D., SOCHEN N., SCHNORR C., "A multiphase dynamic labeling model for variational recognition-driven image segmentation", *International Journal of Computer Vision*, vol. 66, no. 1, pp. 67–81, 2006.

[DEL 01] DELFOUR M., ZOLÉSIO J.-P., *Shapes and Geometries*, Advances in Design and Control, SIAM, 2001.

[DEL 06] DELYON G., GALLAND F., REFREGIER P., "Minimal stochastic complexity image partitioning with unknown noise model", *IEEE Transactions on Image Processing*, vol. 15, no. 10, pp. 3207–3212, 2006.

[DES 11] DESQUESNES X., ELMOATAZ A., LEZORAY O., "PDEs level sets on weighted graphs", *International Conference on Image Processing*, pp. 3377–3380, 2011.

[DIE 12] DIETENBECK T., ALESSANDRINI M., BARBOSA D.C. *et al.*, "Detection of the whole myocardium in 2D-echocardiography for multiple orientations using a geometrically constrained level-set", *Medical Image Analysis*, vol. 16, no. 2, pp. 386–401, 2012.

[DIE 13] DIETENBECK T., BARBOSA D., ALESSANDRINI M. *et al.*, "Multiview myocardial tracking in echocardiographic 2D sequences using shape and motion constrained level-set", *IEEE International Symposium on Biomedical Imaging (ISBI)*, pp. 1010–1013, 2013.

[DUA 08] DUAN Q., ANGELINI E., HOMMA S. *et al.*, "Real-time segmentation of 4D ultrasound by active geometric functions", *International Symposium on Biomedical Imaging (ISBI)*, pp. 233–236, 2008.

[DUA 10] DUAN Q., ANGELINI E.D., LAINE A.F., "Real-time segmentation by Active Geometric Functions", *Computer Methods and Programs in Biomedicine*, vol. 98, no. 3, pp. 223–230, 2010.

[DYD 06] DYDENKO I., JAMAL F., BERNARD O. *et al.*, "A level set framework with a shape and motion prior for segmentation and region tracking in echocardiography", *Medical Image Analysis*, vol. 10, no. 2, pp. 162–177, 2006.

[EHR 08] EHRHARDT J., SCHMIDT-RICHBERG A., HANDELS H., "Simultaneous segmentation and motion estimation in 4D CT data using a variational approach", *SPIE Medical Imaging*, vol. 6914, pp. 37.1–37.10, 2008.

[ELM 08] ELMOATAZ A., LEZORAY O., BOUGLEUX S., "Nonlocal discrete regularization on weighted graphs: a framework for image and manifold processing", *IEEE Transactions on Image Processing*, vol. 17, no. 7, pp. 1047–1060, 2008.

[EPS 87] EPSTEIN C.L., GAGE M., "The Curve Shortening Flow", CHORIN A., MAJDA A. (eds), *Wave Motion: Theory, Modeling, and Computation*, Mathematical Sciences Research Institute Publications, Springer-Verlag, New York, vol. 7, pp. 15–59, 1987.

[FOU 06] FOULONNEAU A., CHARBONNIER P., HEITZ F., "Affine-invariant geometric shape priors for region-based active contours", *IEEE Transactions on Pattern Analysis and Machine Intelligence*, vol. 28, no. 8, pp. 1352–1357, 2006.

[GEL 07] GELAS A., BERNARD O., FRIBOULET D. *et al.*, "Compactly supported radial basis functions based collocation method for level-set evolution in image segmentation", *IEEE Transactions on Image Processing*, vol. 16, no. 7, pp. 1873–1887, 2007.

[GON 04] GONG L., PATHAK S., HAYNOR D. *et al.*, "Parametric shape modeling using deformable superellipses for prostate segmentation", *IEEE Transactions on Medical Imaging*, vol. 23, no. 3, pp. 340–349, 2004.

[GRA 08] GRADY L., ALVINO C., "Reformulating and optimizing the Mumford-Shah functional on a graph – a faster, lower energy solution", *ECCV*, pp. 248–261, 2008.

[GRA 09] GRADY L., ALVINO C., "The piecewise smooth Mumford-Shah functional on an arbitrary graph", *IEEE Transactions on Image Processing*, vol. 18, pp. 2547–2561, 2009.

[HAM 10] HAMOU A., EL-SAKKA M., "Optical flow active contours with primitive shape priors for echocardiography", *EURASIP Journal of Advances in Signal Processing*, vol. 21, pp. 1–11, 2010.

[HEN 13] HENNEMUTH A., FRIMAN O., HUELLEBRAND M. *et al.*, "Mixture-model-based segmentation of myocardial delayed enhancement MRI", CAMARA O., MANSI T., POP M. *et al.*, (eds), *Statistical Atlases and Computational Models of the Heart. Imaging and Modelling Challenges*, vol. 7746, Lecture Notes in Computer Science, pp. 87–96, Springer, Berlin-Heidelberg, 2013.

[HER 04] HERBULOT A., JEHAN-BESSON S., BARLAUD M. *et al.*, "Shape gradient for image segmentation using information theory", *IEEE International Conference on Acoustics, Speech, and Signal Processing (ICASSP)*, vol. 3, pp. 21–24, 2004.

[HER 06] HERBULOT A., JEHAN-BESSON S., DUFFNER S. *et al.* "Segmentation of vectorial image features using shape gradients and information measures", *Journal of Mathematical Imaging and Vision*, vol. 25, no. 3, pp. 365–386, 2006.

[HSU 06a] HSU L.-Y., INGKANISORN W.P., KELLMAN P., *et al.*, "Quantitative myocardial infarction on delayed enhancement MRI. Part II: Clinical application of an automated feature analysis and combined thresholding infarct sizing algorithm", *Journal of Magnetic Resonance Imaging*, John Wiley & Sons, New York, vol. 23, no. 3, pp. 309–314, 2006.

[HSU 06b] HSU L.-Y., NATANZON A., KELLMAN P. *et al.*, "Quantitative myocardial infarction on delayed enhancement MRI. Part I: Animal validation of an automated feature analysis and combined thresholding infarct sizing algorithm", *Journal of Magnetic Resonance Imaging*, John Wiley & Sons, New York, vol. 23, no. 3, pp. 298–308, 2006.

[JAC 99] JACOB G., NOBLE J., MULET-PARADA M. *et al.*, "Evaluating a robust contour tracker on echocardiographic sequences", *Medical Image Analysis*, vol. 3, no. 1, pp. 63–75, 1999.

[JAI 96] JAIN A.K., ZHONG Y., LAKSHMANAN S., "Object matching using deformable templates", *IEEE Transactions on Pattern Analysis and Machine Intelligence*, vol. 18, no. 3, pp. 267–278, 1996.

[JAI 98] JAIN A.K., ZHONG Y., DUBUISSON-JOLLY M.-P., "Deformable template models: A review", *Signal Processing*, vol. 71, no. 2, pp. 109–129, 1998.

[JEH 03] JEHAN-BESSON S., BARLAUD M., AUBERT G., "DREAM2S: deformable regions driven by an Eulerian accurate minimization method for image and video segmentation", *International Journal of Computer Vision*, vol. 53, no. 1, pp. 45–70, 2003.

[JUN 05] JUNMO K., FISHER J.W., YEZZI A., *et al.*, "A nonparametric statistical method for image segmentation using information theory and curve evolution", *IEEE Transactions on Image Processing*, vol. 14, no. 10, pp. 1486–1502, 2005.

[KAC 08] KACHENOURA N., REDHEUIL A., HERMENT A., *et al.*, "Robust assessment of the transmural extent of myocardial infarction in late gadolinium-enhanced MRI studies using appropriate angular and circumferential subdivision of the myocardium", *European Radiology*, Springer-Verlag, vol. 18, no. 10, pp. 2140–2147, 2008.

[KAN 12] KANG D., WOO J., SLOMKA P.J. *et al.*, "Heart chambers and whole heart segmentation techniques: review", *Journal of Electronic Imaging*, vol. 21, no. 1, pp. 010901.1–010901.16, 2012.

[KAS 88] KASS M., WITKIN A., TERZOPOULOS D., "Snakes: active contour models", *International Journal of Computer Vision*, vol. 1, pp. 321–331, 1988.

[KOH 06] KOHLBERGER T., CREMERS D., ROUSSON M. *et al.*, "4D shape priors for a level set segmentation of the left myocardium in SPECT sequences", *Medical Image Computing and Computer-Assisted Intervention (MICCAI)*, pp. 92–100, 2006.

[LAC 05] LACHAUD J., TATON B., "Deformable model with a complexity independent from image resolution", *Computer Vision and Image Understanding*, vol. 99, no. 3, pp. 453–475, 2005.

[LAN 08] LANKTON S., TANNENBAUM A., "Localizing region-based active contours", *IEEE Transactions on Image Processing*, vol. 17, no. 11, pp. 2029–2039, 2008.

[LEC 09] LECELLIER F., JEHAN-BESSON S., FADILI J. *et al.*, "Optimization of divergences within the exponential family for image segmentation", *Scale Space and Variational Methods in Computer Vision, Second International Conference, SSVM 2009, Voss, Norway*, vol. 5567, Lecture Notes in Computer Science, pp. 137–149, 2009.

[LEC 10] LECELLIER F., FADILI J., JEHAN-BESSON S. *et al.*, "Region-based active contours with exponential family observations", *Journal of Mathematical Imaging and Vision*, vol. 36, no. 1, pp. 28–45, 2010.

[LEU 10] LEUNG K.Y.E., BOSCH J.G., "Automated border detection in three-dimensional echocardiography: principles and promises", *European Journal of Echocardiography*, vol. 11, no. 2, pp. 97–108, 2010.

[LEU 11] LEUNG K.Y.E., DANILOUCHKINE M.G., VAN STRALEN M. *et al.*, "Left ventricular border tracking using cardiac motion models and optical flow", *Ultrasound in Medicine and Biology*, vol. 37, no. 4, pp. 605–616, 2011.

[LEV 00] LEVENTON M.E., GRIMSON W.E.L., FAUGERAS O., "Statistical shape influence in geodesic active contours", *IEEE Conference on Computer Vision and Pattern Recognition (CVPR)*, vol. 1, pp. 316–323, 2000.

[LI 05] LI C., XU C., GUI C. *et al.*, "Level set evolution without re-initialization: a new variational formulation", *Computer Vision and Pattern Recognition*, vol. 1, pp. 430–436, 2005.

[LI 08] LI C., CHIU-YEN K., GORE J.C. *et al.*, "Minimization of region-scalable fitting energy for image segmentation", *IEEE Transactions on Image Processing*, vol. 17, no. 10, pp. 1940–1949, 2008.

[LIN 03] LIN N., PAPADEMETRIS X., SINUSAS A. *et al.*, "Analysis of left ventricular motion using a general robust point matching algorithm", *Medical Image Computing and Computer-Assisted Intervention – MICCAI 2003*, pp. 556–563, 2003.

[LO 10] LO P.C.P., Segmentation of Lung Structures in CT, PhD, University of Copenhagen, 2010.

[LYN 06] LYNCH M., GHITA O., WHELAN P.F., "Left-ventricle myocardium segmentation using a coupled level-set with a priori knowledge", *Computerized Medical Imaging and Graphics*, vol. 30, no. 4, pp. 255–262, 2006.

[LYN 08] LYNCH M., GHITA O., WHELAN P.F., "Segmentation of the left ventricle of the heart in 3-D+t MRI data using an optimized nonrigid temporal model", *IEEE Transactions on Medical Imaging*, vol. 27, no. 2, pp. 195–203, 2008.

[MAL 95] MALLADI R., SETHIAN J., VEMURI B., "Shape modeling with front propagation: a level set approach", *IEEE Transactions on Pattern Analysis and Machine Intelligence*, vol. 17, no. 2, pp. 158–175, 1995.

[MAL 99] MALASSIOTIS S., STRINTZIS M., "Tracking the left ventricle in echocardiographic images by learning heart dynamics", *IEEE Transactions on Medical Imaging*, vol. 18, no. 3, pp. 282–290, 1999.

[MAR 00] MARQUINA A., OSHER S., "Explicit algorithms for a new time dependent model based on level set motion for nonlinear deblurring and noise removal", *SIAM Journal on Scientific Computing*, vol. 22, pp. 387–405, 2000.

[MAR 06] MARTIN P., REFREGIER P., GALLAND F. *et al.*, "Nonparametric statistical snake based on the minimum stochastic complexity", *IEEE Transactions on Image Processing*, vol. 15, no. 9, pp. 2762–2770, 2006.

[MAT 06] MATTHEW H., "First order geometric distance (the myth of Sampsonus)", *British Machine Vision Conference*, vol. 1, pp. 87–96, 2006.

[MIL 09] MILLE J., "Narrow band region-based active contours and surfaces for 2D and 3D segmentation", *Computer Vision and Image Understanding*, vol. 113, no. 9, pp. 946–965, 2009.

[MIT 02] MITCHELL S.C., BOSCH J.G., LELIEVELDT B.P.F. *et al.*, "3-D active appearance models: segmentation of cardiac MR and ultrasound images", *IEEE Transactions on Medical Imaging*, vol. 21, no. 9, pp. 1167–1178, 2002.

[MUL 00] MULET-PARADA M., NOBLE J., "2D+T acoustic boundary detection in echocardiography", *Medical Image Analysis*, vol. 4, no. 1, pp. 21–30, 2000.

[NIK 06] NIKOLOVA M., ESEDOGLU S., CHAN T.F., "Algorithms for finding global minimizers of image segmentation and denoising models", *SIAM Journal of Applied Mathematics*, vol. 66, no. 5, pp. 1632–1648, 2006.

[NOB 06] NOBLE J., BOUKERROUI D., "Ultrasound image segmentation: a survey", *IEEE Transactions on Medical Imaging*, vol. 25, no. 8, pp. 987–1010, 2006.

[ORD 08] ORDERUD F., RABBEN S.I., "Real-time 3D segmentation of the left ventricle using deformable subdivision surfaces", *IEEE Conference on Computer Vision and Pattern Recognition (CVPR)*, pp. 1–8, 2008.

[OSH 88] OSHER S., SETHIAN J., "Fronts propagating with curvature-dependent speed: algorithms based on Hamilton-Jacobi formulations", *Journal of Computational Physics*, vol. 79, no. 1, pp. 12–49, 1988.

[OSH 02] OSHER S., FEDKIW R., *Level Set Methods and Dynamic Implicit Surfaces*, Springer, Berlin, 2002.

[OSH 03] OSHER S., PARAGIOS N., *Geometric Level Set Methods in Imaging, Vision and Graphics*, Springer, Berlin, 2003.

[PAP 00] PAPIN C., BOUTHEMY P., MÉMIN E., ROCHARD G., "Tracking and characterization of highly deformable cloud structures", *European Conference on Computer Vision (ECCV)*, pp. 428–442, 2000.

[PAP 08] PAPADAKIS N., MÉMIN E., "A variational technique for time consistent tracking of curves and motion", *Journal of Mathematical Imaging and Vision*, vol. 31, no. 1, pp. 81–103, 2008.

[PAR 02] PARAGIOS N., ROUSSON M., RAMESH V., "Matching distance functions: a shape-to-area variational approach for global-to-local registration", *European Conference on Computer Vision – ECCV*, Springer-Verlag, pp. 775–789, 2002.

[PAR 04] PARAGIOS N., MELLINA-GOTTARDO O., RAMESH V., "Gradient vector flow fast geometric active contours", *IEEE Transactions on Pattern Analysis and Machine Intelligence*, vol. 26, no. 3, pp. 402–407, 2004.

[PAR 05a] PARAGIOS N., JOLLY M., TARON M. *et al.*, "Active shape models & segmentation of the left ventricle in echocardiography", *International Conference on Scale Space Theories and PDEs methods in Computer Vision*, pp. 131–142, 2005.

[PAR 05b] PARAGIOS N., DERICHE R., "Geodesic active regions and level set methods for motion estimation and tracking", *Computer Vision and Image Understanding*, vol. 97, no. 3, pp. 259–282, 2005.

[PEN 99] PENG D., MERRIMAN B., OSHER S., ZHAO H., KANG M., "A PDE-based fast local level set method", *Journal of Computational Physics*, vol. 155, no. 2, pp. 410–438, 1999.

[PET 11] PETITJEAN C., DACHER J.-N., "A review of segmentation methods in short axis cardiac MR images", *Medical Image Analysis*, vol. 15, no. 2, pp. 169–184, 2011.

[POS 05] POSITANO V., PINGITORE A., GIORGETTI A. *et al.*, "A fast and effective method to assess myocardial necrosis by means of contrast magnetic resonance imaging", *Journal of Cardiovascular Magnetic Resonance*, Informa UK, vol. 7, no. 2, pp. 48–494, 2005.

[RAD 09] RADAU P., LU Y., CONNELLY K. *et al.*, "Evaluation framework for algorithms segmenting short axis cardiac MRI", *MIDAS Journal – Cardiac MR Left Ventricle Segmentation Challenge*, vol. 1, pp. 1–7, 2009.

[RAM 10] RAMUS L., THARIAT J., MARCY P.Y. *et al.*, "Outils de contourage, utilisation et construction d'atlas anatomiques: exemples des cancers de la tête et du cou", *Cancer/Radiothérapie*, vol. 14, no. 3, pp. 206–212, 2010.

[REM 04] REMME E.W., YOUNG A.A., AUGENSTEIN K.F. *et al.*, "Extraction and quantification of left ventricular deformation modes", *IEEE Transactions on Biomedical Engineering*, vol. 51, no. 11, pp. 1923–1931, 2004.

[ROH 05] ROHLFING T., BRANDT R., MENZEL R. *et al.*, *Quo Vadis, Atlas-Based Segmentation?*, pp. 435–486, Topics in Biomedical Engineering, International Book Series, Springer US, 2005.

[RON 94] RONFARD R., "Region-based strategies for active contour models", *International Journal of Computer Vision*, vol. 13, no. 2, pp. 229–251, 1994.

[ROU 02] ROUSSON M., PARAGIOS N., "Shape priors for level set representations", *European Conference on Computer Vision – ECCV*, Springer-Verlag, pp. 78–92, 2002.

[ROU 04] ROUSSON M., PARAGIOS N., DERICHE R., "Implicit active shape models for 3D segmentation in MR imaging", *Medical Image Computing and Computer-Assisted Intervention – MICCAI 2004*, Springer, Berlin-Heidelberg, pp. 209–216, 2004.

[RUE 97] RUECKERT D., BURGER P., "Shape-based segmentation and tracking in 4D cardiac MR images", TROCCAZ J., GRIMSON E., MÖSGES R. (eds), *CVRMed-MRCAS'97*, vol. 1205, Springer, Berlin-Heidelberg, pp. 43–52, 1997.

[SAM 82] SAMPSON P.D., "Fitting conic sections to "very scattered" data: An iterative refinement of the bookstein algorithm", *Computer Graphics and Image Processing*, vol. 18, no. 1, pp. 97–108, 1982.

[SAR 05] SARTI A., CORSI C., MAZZINI E. *et al.*, "Maximum likelihood segmentation of ultrasound images with Rayleigh distribution", *IEEE Transactions on Ultrasonics, Ferroelectricity and Frequency Control*, vol. 52, no. 6, pp. 947–960, 2005.

[SAR 08] SAROUL L., BERNARD O., VRAY D., *et al.*, "Prostate segmentation in echographic images: a variational approach using deformable super-ellipse and Rayleigh distribution", *International Symposium on Biomedical Imaging (ISBI)*, pp. 129–132, 2008.

[SCH 08] SCHAERER J., Segmentation et suivi de structures par modèle déformable élastique non-linéaire. Application à l'analyse automatisée de séquences d'IRM cardiaques, Thesis, INSA, Lyon, 2008.

[SCH 10] SCHAERER J., CASTA C., POUSIN J. *et al.*, "A dynamic elastic model for segmentation and tracking of the heart in MR image sequences", *Medical Image Analysis*, vol. 14, no. 6, pp. 738–749, 2010.

[SCL 95] SCLAROFF S., PENTLAND A., "Modal matching for correspondence and recognition", *IEEE Transactions on Pattern Analysis and Machine Intelligence*, vol. 17, no. 6, pp. 545–561, 1995.

[SLU 06] SLUIMER I., SCHILHAM A., PROKOP M. *et al.*, "Computer analysis of computed tomography scans of the lung: a survey", *IEEE Transactions on Medical Imaging*, vol. 25, no. 4, pp. 385–405, 2006.

[SOK 92] SOKOLOWSKI J., ZOLÉSIO J.-P., *Introduction to shape optimization. Shape sensitivity analysis*, vol. 16, Series in Computational Mathematics, Springer-Verlag, Berlin, 1992.

[STO 12] STOICA R., POUSIN J., CASTA C. *et al.*, "Integrating fiber orientation constraint into a spatio-temporal FEM model for heart borders and motion tracking in dynamic MRI", *Statistical Atlases and Computational Models of the Heart: Imaging and Modelling Challenges, MICCAI STACOM Workshop*, 2012.

[SUR 02] SURI J., LIU K., SINGH S. *et al.*, "Shape recovery algorithms using level sets in 2-D/3-D medical imagery: a state-of-the-art review", *IEEE Transactions on Information Technology in Biomedicine*, vol. 6, no. 1, pp. 8–28, 2002.

[SUS 99] SUSSMAN M., FATEMI E., "An efficient, interface-preserving level set redistancing algorithm and its application to interfacial incompressible fluid flow", *SIAM Journal on Scientific Computing*, vol. 20, no. 4, pp. 1165–1191, 1999.

[TA 01] TA V.-T., ELMOATAZ A., LEZORAY O., "Nonlocal PDEs-based morphology on weighted graphs for image and data processing", *IEEE Transactions on Image Processing*, vol. 20, no. 6, pp. 1504–1516, 2001.

[TAO 07] TAO Z., TAGARE H.D., "Tunneling descent for m.a.p. active contours in ultrasound segmentation", *Medical Image Analysis*, vol. 11, no. 3, pp. 266–281, 2007.

[TSA 03a] TSAI A., YEZZI A., WELLS W. *et al.*, "A shape-based approach to the segmentation of medical imagery using level sets", *IEEE Transactions on Medical Imaging*, vol. 22, no. 2, pp. 137–154, 2003.

[TSA 03b] TSAI R., OSHER S., "Level set methods and their applications in image science", *Communications in Mathematical Sciences*, vol. 1, no. 4, pp. 1–20, 2003.

[UNA 05] UNAL G., KRIM H., YEZZI A., "Fast incorporation of optical fow into active polygons", *IEEE Transactions on Image Processing*, vol. 14, no. 6, pp. 745–759, 2005.

[VAL 06] VALLET B., ANGELINI E.D., LAINE A.F., "Variational segmentation framework in prolate spheroidal coordinates for 3D real-time echocardiography", *SPIE Medical Imaging*, vol. 6144, pp. 1370–1380, 2006.

[VAL 11] VALINDRIA V.V., ANGUE M., VIGNON N. *et al.*, "Automatic quantification of myocardial infarction from delayed enhancement MRI", *Signal-Image Technology and Internet-Based Systems (SITIS), 2011 Seventh International Conference*, pp. 277–283, 2011.

[VAN 12] VANDEMEULEBROUCKE J., BERNARD O., RIT S. *et al.*, "Automated segmentation of a motion mask to preserve sliding motion in deformable registration of thoracic CT", *Medical Physics*, vol. 39, no. 2, pp. 1006–1015, 2012.

[VIN 99] VINCENT F., CLARYSSE P., CROISILLE P. *et al.*, "Segmentation et suivi de mouvement d'objets déformables par région active", *GRETSI'99*, pp. 163–166, 1999.

[VIN 00] VINCENT F., CLARYSSE P., CROISILLE P. *et al.*, "Segmentation of the heart from MR image sequences using a 3D active model", *Biomedical Engineering Society Annual Meeting*, 2000.

[VIN 01] VINCENT F., Gabarits déformables élastiques pour la segmentation et le suivi de mouvement du coeur en Imagerie par Résonance Magnétique, Thesis, INSA, Lyon, 2001.

[WOJ 10] WOJAK J., Analyse d'images multimodales TEP-TDM du thorax. Application à l'oncologie: segmentation de tumeurs, organes à risque et suivi longitudinal pour la radiothérapie, Thesis, Télécom ParisTech, December 2010.

[XU 98] XU C., PRINCE J., "Snakes, shapes and gradient vector flow", *IEEE Transactions on Image Processing*, vol. 7, no. 3, pp. 359–369, March 1998.

[YEZ 97] YEZZI A., KICHENASSAMY S., KUMAR A. *et al.*, "A geometric snake model for segmentation of medical imagery", *IEEE Transactions on Medical Imaging*, vol. 16, no. 2, pp. 199–209, 1997.

[YEZ 02] YEZZI A., TSAI A., WILLSKY A., "A fully global approach to image segmentation via coupled curve evolution equations", *Journal of Visual Communication and Image Representation*, vol. 13, nos. 1–2, pp. 195–216, 2002.

[YUI 91] YUILLE A.L., "Deformable templates for face recognition", *Journal of Cognitive Neuroscience*, vol. 3, no. 1, pp. 59–70, 1991.

[ZHA 96] ZHAO H., CHAN T., MERRIMAN B. *et al.*, "A variational level set approach to multiphase motion", *Journal of Computational Physics*, vol. 127, no. 127, pp. 179–195, 1996.

[ZHA 04] ZHANG D., LU G., "Review of shape representation and description techniques", *Pattern Recognition*, vol. 37, no. 1, pp. 1–19, 2004.

[ZHA 05] ZHANG Q., PLESS R., "Segmenting cardiopulmonary images using manifold learning with level sets", *Computer Vision for Biomedical Image Applications*, vol. 3765, pp. 479–488, 2005.

[ZHU 96] ZHU S.C., YUILLE A., "Region competition: unifying snakes, region growing, and Bayes/MDLfor multiband image segmentation", *IEEE Transactions on Pattern Analysis and Machine Intelligence*, vol. 18, no. 9, pp. 884–900, 1996.

[ZHU 07] ZHU Y., PAPADEMETRIS X., SINUSAS A. *et al.*, "Segmentation of myocardial volumes from real-time 3D echocardiography using an incompressibility constraint", *Medical Image Computing and Computer-Assisted Intervention (MICCAI)*, pp. 44–51, 2007.

[ZHU 10] ZHU Y., PAPADEMETRIS X., SINUSAS A. *et al.*, "A coupled deformable model for tracking myocardial borders from real-time echocardiography using an incompressibility constraint", *Medical Image Analysis*, vol. 14, no. 3, pp. 429–448, 2010.